ADVANCING EARTH AND SPACE SCIENCE

Water Resources Research

RESEARCH ARTICLE
10.1029/2021WR031399

Analysis of Surface Water Trends for the Conterminous United States Using MODIS Satellite Data, 2003–2019

Roy E. Petrakis[1], Christopher E. Soulard[2], Eric K. Waller[3], and Jessica J. Walker[1]

[1]U.S. Geological Survey, Western Geographic Science Center, Tucson, AZ, USA, [2]U.S. Geological Survey, Western Geographic Science Center, Moffett Field, CA, USA, [3]Contractor to the U.S. Geological Survey, Western Geographic Science Center, Portland, OR, USA

Key Points:

- Monthly Moderate Resolution Imaging Spectroradiometer maps can be used to calculate and compare surface water area trends across US ecoregions
- The central United States (US) underwent an increase in surface water while most of the western/eastern US underwent a decline from 2003 through 2019
- Monthly trends in surface water were congruent with monthly trends in discharge for the majority of Level III Ecoregions in the US

Correspondence to:

R. E. Petrakis,
rpetrakis@usgs.gov

Citation:

Petrakis, R. E., Soulard, C. E., Waller, E. K., & Walker, J. J. (2022). Analysis of surface water trends for the conterminous United States using MODIS satellite data, 2003–2019. *Water Resources Research*, *58*, e2021WR031399. https://doi.org/10.1029/2021WR031399

Received 12 OCT 2021
Accepted 6 JUN 2022

Author Contributions:

Conceptualization: Roy E. Petrakis, Christopher E. Soulard, Eric K. Waller, Jessica J. Walker
Formal analysis: Roy E. Petrakis, Christopher E. Soulard, Eric K. Waller
Methodology: Roy E. Petrakis, Christopher E. Soulard, Eric K. Waller, Jessica J. Walker
Project Administration: Christopher E. Soulard
Software: Roy E. Petrakis, Christopher E. Soulard, Eric K. Waller, Jessica J. Walker
Supervision: Christopher E. Soulard

Abstract Satellite imagery is commonly used to map surface water extents over time, but many approaches yield discontinuous records resulting from cloud obstruction or image archive gaps. We applied the Dynamic Surface Water Extent (DSWE) model to downscaled (250-m) daily Moderate Resolution Imaging Spectroradiometer (MODIS) data in Google Earth Engine to generate monthly surface water maps for the conterminous United States (US) from 2003 through 2019. The aggregation of daily observations to monthly maps of maximum water extent produced records with diminished cloud and cloud shadow effects across most of the country. We used the continuous monthly record to analyze spatiotemporal surface water trends stratified within Environmental Protection Agency Ecoregions. Although not all ecoregion trends were significant ($p < 0.05$), results indicate that much of the western and eastern US underwent a decline in surface water over the 17-year period, while many ecoregions in the Great Plains had positive trends. Trends were also generated from monthly streamgage discharge records and compared to surface water trends from the same ecoregion. These approaches agreed on the directionality of trend detected for 54 of 85 ecoregions, particularly across the Great Plains and portions of the western US, whereas trends were not congruent in select western deserts, the Great Lakes region, and the southeastern US. By describing the geographic distribution of surface water over time and comparing these records to instrumented discharge data across the conterminous US, our findings demonstrate the efficacy of using satellite imagery to monitor surface water dynamics and supplement traditional instrumented monitoring.

Plain Language Summary Daily satellite images can be used to create cloud-free maps of surface water for most of the United States (US). An analysis of these maps over multiple decades reveals surface water change in large-scale water features such as lakes, reservoirs, and major rivers. Results show that increasing surface water trends are more common across the central US while decreasing trends are present across much of the western and eastern regions over the past 17 years. More specifically, we observed certain seasonal trends including increasing spring flooding along the Mississippi River. Comparing these data to trends in streamgage discharge provides additional insights into certain regions where surface water changes are more directly related to dynamic surface water flows. Results from this study identify national and regional surface water variability over space and time that can contribute to more effective water resource management.

1. Introduction

1.1. The Purpose of Measuring Surface Water

Understanding the spatial and temporal dynamics of surface water extent is essential for water management planning and for monitoring drought and flood events. For instance, dam release schedules may take into account historical reservoir water levels and past responses to major precipitation events, while adjusting for active water resource needs (Bureau of Reclamation, 2020; Pulwarty & Melis, 2001). Daily streamflow data have been used to build a comprehensive multi-decadal record of droughts in the conterminous United States (hereafter US) (Austin et al., 2017; Zou et al., 2018). Investigations of surface water peaks over time may also help construct flood chronologies (Smith et al., 2018). Flooding has caused major monetary impacts across the US over the past century (Downton et al., 2005); identifying the patterns and causes of flooding can help estimate future damages (Wobus et al., 2014). While the U.S. Geological Survey (USGS) maintains streamgages that sample representative locations to support regional water management, flood forecasting, and trend detection (National Research Council, 2004), measurements from discrete locations may not provide a complete picture of surface

Validation: Roy E. Petrakis, Christopher E. Soulard
Visualization: Roy E. Petrakis, Jessica J. Walker
Writing – original draft: Roy E. Petrakis, Christopher E. Soulard, Eric K. Waller, Jessica J. Walker

water and the spatial extent of change. The use of Earth observation satellites to create maps of surface water change is becoming more common for training and validating flood inundation predictions and generating broad insights into surface water dynamics (Bales & Wagner, 2009; Pickens et al., 2020). Progress is being made to generate spatially explicit, wall-to-wall time series of surface water, but to date, map data with sufficient spatial and temporal resolutions to monitor long-term surface water dynamics, event-driven changes, and corresponding change drivers remain limited (Tulbure & Broich, 2019).

Surface water management requires long-term, regional-scale approaches because the rates and causes of surface water change vary substantially among geographic areas (Müller Schmied et al., 2016). Human water demands (i.e., for agriculture and irrigation, water purveyance, power and industry, mining, and domestic use), land use/land cover (LULC) change, and weather (i.e., precipitation intensity and duration, temperature, and solar radiation) influence surface water change differently across landscapes over time (Dieter et al., 2017; Karl & Riebsame, 1989; Krueger et al., 2017; Pimentel et al., 1997; Poff et al., 2006; Slater & Villarini, 2017). Consequently, surface water fluctuations may simultaneously vary between regions, where declines may trigger rationing in one part of the country and sudden increases may create floods and economic losses elsewhere. The magnitude and location of ecosystem impacts can also be complex (Schaffer-Smith et al., 2017). In both cases, surface water maps can be employed to identify the spatial and temporal dynamics of surface water and be fed into LULC change forecasts to model the impact of surface water change across different landscapes (Garen, 1993; Shuter et al., 2013).

1.2. Status of Surface Water Mapping Research

Large-area surface water mapping has grown over the past decade with the increase in remote sensing capabilities, expanded access to satellite imagery sources (Zhou et al., 2017), and the advent of cloud-computing environments. On the Google Earth Engine (GEE) cloud platform (Gorelick et al., 2017) water-related applications represent the second largest field of exploration (Tamiminia et al., 2020). These developments have broadened the spatial and temporal scope of viable research objectives and data products. Even moderate-resolution imagery can be scaled globally, such as the European Commission's Joint Research Center (JRC) Global Surface Water Extent dataset, a Landsat-based approach at 30 m for generating monthly, multi-decadal surface water mapping (Pekel et al., 2016). The assembly of dense image time-series allows researchers to track change over time, from mapping the extents of global reservoirs (Khandelwal et al., 2017; Rad et al., 2021) to develop global water bodies maps that distinguish dynamic and static water areas (Yamazaki et al., 2015). US-focused efforts include measuring regional interannual trends of annual surface water at 30 m across the nation from 1984 through 2016 (Zou et al., 2018).

1.3. Quantifying Surface Water With the DSWE Algorithm

Methods of identifying surface water through satellite image interpretation vary. The focus of this paper is the Dynamic Surface Water Extent (DSWE) model, a decision-tree classification originally developed to map surface water in 30-m Landsat satellite imagery (Jones, 2015, 2019). Efforts to implement the DSWE model based on the Landsat archive in GEE include the Central Valley of California (Walker, Soulard, et al., 2020), Cambodia (Soulard et al., 2020), and the Mid-Atlantic region of the United States (Vanderhoof et al., 2020). DSWE has also been combined with the JRC product to compute probabilities of open water to help classify surface inundation during flood events based on Sentinel-1 data (DeVries et al., 2020). With the public availability of JavaScript algorithm code specific to GEE (Walker, Petrakis, et al., 2020), DSWE implementation can be customized for unique surface water applications and different satellite sensors. While DSWE maps at 30 m resolution are useful for identifying changes in moderate-scale water features, the 16-day revisit time of each Landsat satellite is often insufficient for detecting and analyzing seasonal trends and transient flood events, exacerbated by the frequency of cloudy observations. Additionally, the number of images available within the Landsat archive varies significantly in different parts of the world (Wulder et al., 2016). Daily imagery from Moderate Resolution Imaging Spectroradiometer (MODIS) satellites Terra and Aqua have helped provide a useful alternative to Landsat-based approaches for DSWE mapping, albeit at a coarser 250-m resolution and for a shorter period of availability (2000 to present) (Soulard et al., 2022). The generation of MODIS-based DSWE products ("DSWEmod") for California leveraged daily data to create monthly and sub-monthly surface water maps with substantially reduced cloud obstruction. The contrast in cloud cover between the Landsat DSWE and DSWEmod products for California was most pronounced in the winter months when obscured data averaged 12.4% and 1.4% for the Landsat- and MODIS-derived monthly maps, respectively (Soulard et al., 2022).

1.4. Trends in Surface Water Extent

Many prior studies have used trend analyses to characterize water resources over multiple time intervals (i.e., seasonal, annual, and multi-year) and have identified aspects of water presence over time, such as droughts, flood frequency, and general patterns of streamflow, which can have implications for resource management decisions (Kunkel et al., 1999; Lins & Slack, 1999; Milano et al., 2013; Miller & Piechota, 2011; Webb & Nobilis, 1995). Temporal variability within trend analyses is also revealing; longer intervals can capture major trends while shorter intervals may identify acute flooding and other ephemeral changes. However, data continuity is paramount in trend analysis, and techniques aiming to test the temporal limits of trend analysis using optical imagery data must measure the influence of cloud obstruction in creating data gaps. Soulard et al. (2022) concluded that complete, cloud-free monthly records spanning multiple decades represent a reasonable temporal resolution for applications focused on intra- and inter-annual surface water dynamics. Recent literature suggests that dense time series are well-suited to capture processes of land surface change at monthly scales (Senay et al., 2017; Tulbure & Broich, 2013; Waylen et al., 2014).

Regions across the US have been experiencing unique hydrologic challenges during the early-21st century which may be driving trends in surface water, including an extended and intensifying megadrought across the West (Williams et al., 2020), periodic short-term drought and flood events across the Southeast (Labosier & Quiring, 2013), and increasingly frequent flooding events in the Mississippi River Basin (National Weather Service, 2019). Spatially explicit maps of surface water produced at a monthly scale can capture surface water changes related to these stresses and identify the extent of such changes, an insight that cannot be directly observed using point-based streamgage networks. While optical satellites do have clear limitations, imagery may remain a valuable resource in locations where a sparse distribution of streamgages limits the ability to gather hydrological data.

1.5. Ecoregion Perspective

Surface water extent exhibits considerable spatiotemporal variability across the US (Senay et al., 2017; Tulbure & Broich, 2013; Waylen et al., 2014). Spatial stratification is helpful for conveying region-specific dynamics. Hydrologic Unit Codes (HUCs), which represent hydrologic drainage areas, are often used as a spatial delineation of water resources (Seaber et al., 1987). However, HUCs are not designed for ecological analyses and can span heterogeneous areas (Griffith et al., 1999). The ecoregion framework, in contrast, separates the country into zones of relatively homogenous biotic and abiotic influence, including land use, soil, vegetation, and climate characteristics such as precipitation (Omernik, 1987). While human uses are not accounted for in this framework, and water purveyance (and water cycle teleconnections) often spans multiple regions, an ecoregion approach is generally beneficial for climatic comparisons and is often scalable to land management operations (Omernik & Bailey, 1997).

1.6. Study Objectives

As the MODIS program approaches its third decade in operation, the lengthening time span of the MODIS image archive now allows for the detection of recent ecoregional patterns or trends over large geographic extents. The objectives of this study are to (a) adapt and scale the DSWEmod model of Soulard et al. (2022) to generate monthly surface water products for the conterminous US from 2003 through 2019, (b) analyze the spatial and temporal dynamics of regional surface water extents across the full time series as well as seasonally, and (c) compare surface water area trends to streamgage discharge trends to determine where and how well different approaches to measuring water dynamics align. By reporting surface water change trends at national and regional scales, evaluating how the surface water trend direction compares with discharge records, and summarizing the agreement in trends between the two methodological approaches across ecoregions, we aim to corroborate past findings while also providing new insights into how surface water extents vary over space and time. Ideally, the information provided on the spatial extent of surface water change contained within our analysis will provide regional insights to supplement streamgage data and help land managers more effectively understand

and manage surface waters throughout the US. Further, evaluation of similarities and differences between in-situ and satellite-based observations will help ascertain DSWEmod's efficacy as a tool for monitoring surface water dynamics in parts of the world without streamgage networks.

2. Materials and Methods

2.1. Study Area

To understand the geographic distribution of surface water change across the US, we stratified surface water measurements by Level I and Level III Environmental Protection Agency (EPA) Ecoregions (Omernik, 1987). The 10 Level I Ecoregions are used to provide an overarching summary of change patterns, while the 85 Level III Ecoregions allow us to examine regional variability in more detail (Figure 1). Refer to Figure 1 for numbers, names, and locations of the Level I and Level III Ecoregions listed throughout the text.

2.2. Surface Water Imagery Products

2.2.1. Generation of National-Scale DSWEmod Data

We extended DSWEmod in GEE to create a monthly maximum surface water product for the US from January 2003 through December 2019 (n = 204 months) (Soulard et al., 2021). DSWEmod generation started with pre-processing daily Terra images by performing an angular pixel correction to account for off-nadir viewing angles, applying a collection of standard and customized cloud masks, and downscaling images to create a synthetic 250-m daily product (Schaaf et al., 2002). MODIS Aqua imagery with similar processing was used to help develop the customized cloud masks. Downscaling uses a ratio developed for the near-infrared (NIR) band to apply to the two MODIS short-wave infrared (SWIR) bands, and a ratio developed for the red band to apply to the other MODIS visible channels to generate synthetic 250-m MODIS multispectral data (Nigro et al., 2014). For full image processing details see Soulard et al. (2022).

We applied the DSWEmod algorithm to the processed MODIS data. DSWEmod relies on five water indices created using combinations of the SWIR, NIR, and visible bands: Normalized Difference Vegetation Index (NDVI), Modified Normalized Difference Wetness Index (MNDWI), Automated Water Extent Shadow (AWESH), Multi-band Spectral Relationship Visible (MBSRV), and Multi-Band Spectral Relationship Near-infrared (MBSRN) (USGS, 2019). We generated topographic slope and terrain hillshade products from a digital elevation model (USGS EROS, 2018), with results upscaled to the ~250-m resolution and projection of MODIS data, to screen for steep locations that are unlikely to hold water and shaded pixels that might be misclassified as water. Pixels are categorized according to empirically derived thresholds into one of six classes: not-water (class 0) for clear pixels with no water presence; NoData (class 9) for pixels obscured by clouds, cloud shadow, snow, ice, or hillshade; and four surface water classes, differentiated by confidence level into high-confidence surface water (class 1), moderate-confidence surface water (class 2), potential wetland (class 3), and low-confidence water or wetland (class 4) (USGS, 2019). The monthly surface water product shows the maximum water extent, in which only one surface water detection was necessary across the monthly image composite to classify a pixel as water; the highest confidence surface water class detected at each pixel was used. The lower confidence classes have been shown to misclassify areas with some urban development, considerable vegetation (Soulard et al., 2020; Vanderhoof et al., 2020), and snow. For these reasons, we focused our analysis on the highest-confidence surface water class (DSWEmod class 1, hereafter referred to as "water"), and obscuration from clouds, clouds shadows, and snow/ice collectively (DSWEmod class 9, "NoData").

Images with a large proportion of NoData pixels may result in the reduction of detected water, which may incorrectly suggest that a surface water decline has occurred. Therefore, statistical analyses exclude results from months with greater than 10% NoData area for each Level I and Level III Ecoregion. The 10% threshold was selected to balance data continuity and data contamination. The remaining data were used for the DSWEmod water analysis.

2.2.2. Accuracy Assessment of DSWEmod Water Product

To test the accuracy of DSWEmod at a national scale, we implemented a stratified random sampling approach (Stehman & Foody, 2019) based on Level I Ecoregions; this approach is modeled after Soulard et al. (2022). We selected random samples for each ecoregion within maximum water footprints (1985-2019) determined by an

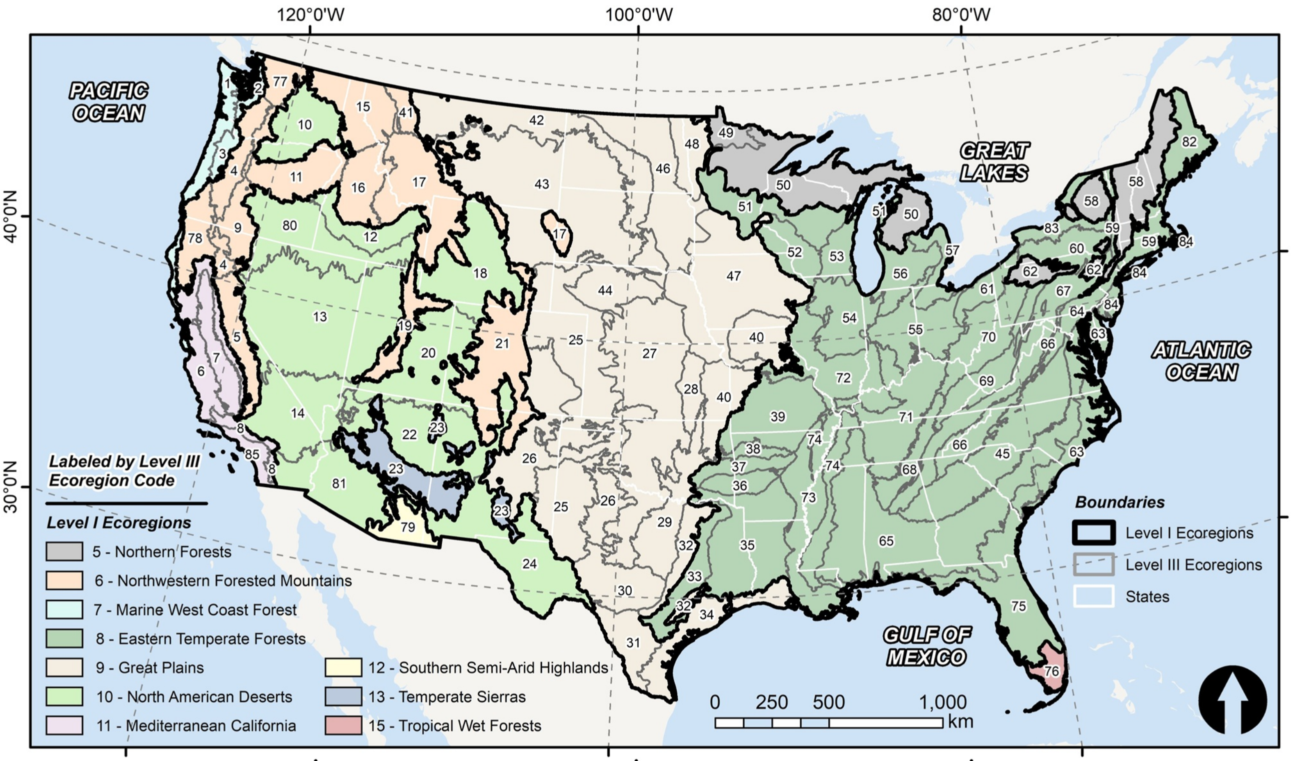

5 – Northern Forests
- 49 – Northern Minnesota Wetlands
- 50 – Northern Lakes and Forests
- 58 – Northeastern Highlands
- 62 – North Central Appalachians

6 – Northwestern Forested Mountains
- 4 – Cascades
- 5 – Sierra Nevada
- 9 – Eastern Cascades Slopes and Foothills
- 11 – Blue Mountains
- 15 – Northern Rockies
- 16 – Idaho Batholith
- 17 – Middle Rockies
- 19 – Wasatch and Uinta Mountains
- 21 – Southern Rockies
- 41 – Canadian Rockies
- 77 – North Cascades
- 78 – Klamath Mountains/California High North Coast Range

7 – Marine West Coast Forest
- 1 – Coast Range
- 2 – Puget Lowland
- 3 – Willamette Valley

8 – Eastern Temperate Forests
- 33 – East Central Texas Plains

Eastern Temperate Forests Cont...
- 35 – South Central Plains
- 36 – Ouachita Mountains
- 37 – Arkansas Valley
- 38 – Boston Mountains
- 39 – Ozark Highlands
- 45 - Piedmont
- 51 – North Central Hardwood Forests
- 52 – Driftless Area
- 53 – Southeastern Wisconsin Till Plains
- 54 – Central Corn Belt Plains
- 55 – Eastern Corn Belt Plains
- 56 – Southern Michigan/Northern Indiana Drift Plains
- 57 – Huron/Erie Lake Plains
- 59 – Northeastern Coastal Zone
- 60 – Northern Allegheny Plateau
- 61 – Erie Drift Plain
- 63 – Middle Atlantic Coastal Plain
- 64 – Northern Piedmont
- 65 – Southeastern Plains
- 66 – Blue Ridge
- 67 – Ridge and Valley
- 68 – Southwestern Appalachians
- 69 – Central Appalachians
- 70 – Western Allegheny Plateau

Eastern Temperate Forests Cont...
- 71 – Interior Plateau
- 72 – Interior River Valleys and Hills
- 73 – Mississippi Alluvial Plain
- 74 – Mississippi Valley Loess Plains
- 75 – Southern Coastal Plain
- 82 – Acadian Plains and Hills
- 83 – Eastern Great Lakes Lowlands
- 84 – Atlantic Coastal Pine Barrens

9 – Great Plains
- 25 – High Plains
- 26 – Southwestern Tablelands
- 27 – Central Great Plains
- 28 – Flint Hills
- 29 – Cross Timbers
- 30 – Edwards Plateau
- 31 – Southern Texas Plains
- 32 – Texas Blackland Prairies
- 34 – Western Gulf Coastal Plain
- 40 – Central Irregular Plains
- 42 – Northwestern Glaciated Plains
- 43 – Northwestern Great Plains
- 44 – Nebraska Sand Hills
- 46 – Northern Glaciated Plains
- 47 – Western Corn Belt Plains

Great Plains Cont...
- 48 – Lake Agassiz Plain

10 – North American Deserts
- 10 – Columbia Plateau
- 12 – Snake River Plain
- 13 – Central Basin and Range
- 14 – Mojave Basin and Range
- 18 – Wyoming Basin
- 20 – Colorado Plateau
- 22 – Arizona/New Mexico Plateau
- 24 – Chihuahuan Deserts
- 80 – Northern Basin and Range
- 81 – Sonoran Basin and Range

11 – Mediterranean California
- 6 – Central California Foothills and Coastal Mountains
- 7 – Central California Valley
- 8 – Southern California Mountains
- 85 – Southern California/Northern Baja Coast

12 – Southern Semi-Arid Highlands
- 79 – Madrean Archipelago

13 – Temperate Sierras
- 23 – Arizona/New Mexico Mountains

15 – Tropical Wet Forests
- 76 – Southern Florida Coastal Plain

Figure 1. Level I and Level III Ecoregions (Omernik, 1987) used as spatial divisions in the analysis. The larger, more generalized Level I Ecoregions are highlighted by bold lines.

independent water product, JRC (Pekel et al., 2016), hereafter referred to as the JRC maximum water stratum. We restricted the accuracy assessment to water bodies greater than 25 ha since 250-m MODIS data cannot adequately resolve smaller features (Jin & Sader, 2005). We also constrained the test to two summer seasons representing the beginning and end of the study period (June through August of 2003 and 2019). We selected summer to maximize the potential for cloud-free image acquisitions across the US since JRC validation data are often incomplete or unavailable for times and locations when clouds are more prevalent. The remaining criteria for selecting samples within the JRC maximum water stratum were that points were at least 100 m inside the edges of water bodies and at least 500 m apart. The sampling procedure produced a wide range of samples between ecoregions based on the relative abundance of large water bodies and the areal extents of each ecoregion. For instance, only nine random samples were selected in the Southern Semi-Arid Highlands (Level I Ecoregion #12), while 6,901 were selected in the Eastern Temperate Forests (#8). All samples were evaluated on both dates.

In addition to JRC maximum water extent serving as the sampling stratum, monthly JRC classifications of surface water presence and absence served as reference data for 2003 and 2019. Global validation results show that monthly JRC products are highly accurate when available (Pekel et al., 2016; Perin et al., 2021), thus justifying use as the best reference data available. We extracted upscaled (resampled from 30 to 250 m) JRC and DSWEmod data at each point location and year. To make the DSWEmod maps comparable to the reference data classes of water/not water/no data, we retained "high confidence" water as an indicator of "water presence" and treated all other classes except for NoData as "water absence". Sample locations were used to construct error matrices for each year of the analysis for the 10 Level I Ecoregions (Congalton, 1991). Only one detection of surface water per year's summer window was required to be classified as either DSWEmod or JRC water. We merged results from each yearly test and calculated the producer's, user's, and overall accuracy.

A qualitative assessment of map products was used to test the ability of the DSWEmod product to resolve spatial detail and detect ephemeral surface water presence across a range of different hydrological features. Our specific objective was to evaluate the capacity of DSWEmod to delineate various hydrological features throughout the year. To accomplish this, we assembled a map of monthly summed water presence (i.e., maximum possible count of 12 at each pixel) for 2019 and identified water features of different widths with consistent surface water presence over time. All monthly maps for the 2019 calendar year were qualitatively compared to high-resolution U.S. Department of Agriculture National Agriculture Imagery Program (NAIP) images (∼1-m spatial resolution) (USDA, 2021) to identify the strengths and limitations of DSWEmod.

2.2.3. Analysis of DSWEmod Seasonal Dynamics

We developed box plots to assess the seasonal and spatial dynamics of DSWEmod water (class 1) and NoData (class 9 – i.e., clouds, cloud shadow, snow, ice, or hillshade) across the US. We calculated the 3-month seasonal mean area of DSWEmod water and NoData nationally for each year from 2003 through 2019, with the seasons defined as winter (December - February), spring (March - May), summer (June - August), and fall (September - November). Given the spread of the winter season across consecutive years, winter averages for 2003 were calculated using only 2 months (i.e., January/February 2003). A companion map was also developed to convey the spatial distribution and frequency of NoData values over the study period. All 204 monthly maps were used to calculate the percentage occurrence of NoData values for each pixel by season.

2.3. Calculation of Surface Water Trends and Descriptive Statistics

We performed Mann-Kendall (M-K) trend tests across multiple time scales for each Level I and Level III Ecoregion using the statistics package R version 4.0.2 (R Core Team, 2020). The M-K test is a non-parametric statistical analysis that detects the presence of consistently increasing or decreasing monotonic trends (Kendall, 1975; Mann, 1945). Adaptations of the test have been widely used in hydrologic time series studies (Yue et al., 2002) since it can tolerate the presence and nonnormal distribution of outliers, such as maximum discharge or flooding events (Hamed, 2008; Villarini et al., 2011, 2012). We quantified seasonal and annual ecoregional mean water area for 2003–2019 (n = 17 records for each season corresponding to the number of years in the study period) and removed sequences with fewer than 10 valid observations (i.e., those meeting our %NoData criterion), which is generally accepted as the minimum number suitable for application of the M-K test (Libiseller & Grimvall, 2002). Analysis at sub-annual intervals is important because climate change is projected to alter the timing of precipitation regimes, storm occurrence, and snowpack accumulation and melting, which may have hydrological implications on a monthly or seasonal basis (Byun et al., 2019). Serial autocorrelation within a time series, independent of sample size, can result in inaccurate rejection of the null hypothesis when using M-K, leading to the incorrect identification of significant trends (Bayazit & Önöz, 2007). Prewhitening can address serial autocorrelation by removing portions of a trend if autocorrelation is present (von Storch, 1999; Yue & Wang, 2002). We used the R "zyp" package (Bronaugh & Werner, 2013) to compute prewhitened linear trends for Level I and Level III Ecoregions and the conterminous US. We applied the Theil-Sen test to each time series to estimate the slope of linear trends (Sen's slope) (Sen, 1968). Whereas M-K provides an estimate of the direction and significance of the monotonic trend, Sen's slope determines an estimate of the rate of the trend in area per unit of time (Banerjee & Kumar, 2018).

As a complement to seasonal and overall M-K trend and Sen's slope analyses, we also summarized each Level I Ecoregion time series using a suite of general statistics over the 2003–2019 study period: (a) mean, minimum, and maximum surface water extent, (b) standard deviation, (c) coefficient of variation, and (d) average percent of ecoregion area across all 204 monthly observations.

2.4. Comparing Surface Water Trends With Instrumented Streamgage Discharge Trends

Trends of instrumented streamgage discharge data are regularly compiled to monitor the flow of surface water across the landscape (Lins & Slack, 1999, 2005; Miller & Piechota, 2011). Discharge has similar driving forces as surface water and its measurement can complement the spatial views of surface water maps generated from satellite imagery (Walker, Soulard, et al., 2020). We compare trends in discharge to trends in surface water for all Level III Ecoregions to assess their agreement (congruence) over the study period across regions. We provide possible explanations for regions where discharge trend direction is not in agreement with the direction of surface water trends (incongruence).

For gage selection and discharge time-series extraction, we utilized the "dataRetrieval" package (DeCicco & Hirsch, 2021) in R, which obtains USGS streamgage time-series data through the National Water Information System (NWIS) (USGS, 2022) service. All available gages were selected within overlapping 8-digit HUCs for each ecoregion and clipped to the respective ecoregion boundary. Additionally, for consideration in this analysis, each gage had to (a) include discharge data (parameter "00060") and (b) have data across >75% of the months of our study period (n = 153 of 204 months). To make the gage sample more comparable to DSWEmod (e.g., moderate-scale water bodies), we only retained gages in each ecoregion where mean annual discharge was in the top three quartiles (i.e., 2–4). Using M-K trend tests, we measured annual discharge trends across all available months, adapting the approach used in Walker, Soulard, et al. (2020) and Soulard et al. (2022). A majority rule was applied to identify the predominant M-K trend direction across all gages tested in each Level III Ecoregion (i.e., increasing or decreasing), and the result was compared to the overall DSWEmod surface water trend derived from the continuous monthly record. Results were mapped across the conterminous US to display patterns of congruency and incongruency in trend direction.

3. Results

3.1. Assessment of DSWEmod for National Applications

3.1.1. Accuracy Assessment With JRC

Contingency matrices were generated for each Level I Ecoregion between 2003 and 2019. To streamline reporting, results from the two tests were added in Table 1 to convey the average mapping accuracy across dates. For the collective summers, overall accuracy exceeds 75% for all tests where a large sample size was available. The exceptions are the Southern Semi-Arid Highlands (Level I Ecoregion #12) and Temperate Sierras (#13) (n < 70 points), where the overall accuracy values were lower. The user's accuracy was greater than producer's accuracy in all ecoregions, and exceeds 90% for 8 of 10 ecoregions, suggesting that there are fewer errors of commission than errors of omission (Table 1).

3.1.2. Delineation of Water Features

We performed qualitative checks against high-resolution, false-color (NIR/red/green) NAIP imagery to investigate how well DSWEmod maps resolve the extent and boundaries of surface water features (Figure 2). Reference

10.1029/2021WR031399

Table 1
Merged Results From the 2003 and 2019 Accuracy Assessments for Each Level I Ecoregion (Omernik, 1987)

Accuracy assessment results					
5—Northern Forests			10—North American deserts		
	JRC Not Water	JRC Water		JRC Not Water	JRC Water
DSWEmod Not Water	156	219	DSWEmod Not Water	723	416
DSWEmod Water	93	4458	DSWEmod Water	43	778
	DSWEmod User's Accuracy = 98.0%			DSWEmod User's Accuracy = 94.8%	
	DSWEmod Producer's Accuracy = 95.3%			DSWEmod Producer's Accuracy = 65.2%	
	Overall Accuracy = 93.7%			Overall Accuracy = 76.6%	
6—Northwestern Forested Mountains			11—Mediterranean California		
	JRC Not Water	JRC Water		JRC Not Water	JRC Water
DSWEmod Not Water	120	199	DSWEmod Not Water	315	112
DSWEmod Water	19	1126	DSWEmod Water	61	302
	DSWEmod User's Accuracy = 98.3%			DSWEmod User's Accuracy = 83.2%	
	DSWEmod Producer's Accuracy = 85.0%			DSWEmod Producer's Accuracy = 72.9%	
	Overall Accuracy = 85.1%			Overall Accuracy = 78.1%	
7—Marine West Coast Forest			12—Southern Semi-Arid Highlands		
	JRC Not Water	JRC Water		JRC Not Water	JRC Water
DSWEmod Not Water	19	26	DSWEmod Not Water	10	7
DSWEmod Water	8	137	DSWEmod Water	0	1
	DSWEmod User's Accuracy = 94.5%			DSWEmod User's Accuracy = 100%	
	DSWEmod Producer's Accuracy = 84.0%			DSWEmod Producer's Accuracy = 12.5%	
	Overall Accuracy = 82.1%			Overall Accuracy = 61.1%	
8—Eastern Temperate Forests			13—Temperate Sierras		
	JRC Not Water	JRC Water		JRC Not Water	JRC Water
DSWEmod Not Water	3856	1637	DSWEmod Not Water	16	16
DSWEmod Water	658	7651	DSWEmod Water	2	30
	DSWEmod User's Accuracy = 92.1%			DSWEmod User's Accuracy = 93.8%	
	DSWEmod Producer's Accuracy = 82.4%			DSWEmod Producer's Accuracy = 65.2%	
	Overall Accuracy = 83.4%			Overall Accuracy = 71.9%	
9—Great Plains			15—Tropical Wet Forests		
	JRC Not Water	JRC Water		JRC Not Water	JRC Water
DSWEmod Not Water	2275	1379	DSWEmod Not Water	365	93
DSWEmod Water	320	5080	DSWEmod Water	37	127
	DSWEmod User's Accuracy = 94.1%			DSWEmod User's Accuracy = 77.4%	
	DSWEmod Producer's Accuracy = 78.6%			DSWEmod Producer's Accuracy = 57.7%	
	Overall Accuracy = 81.2%			Overall Accuracy = 79.1%	

Note. DSWEmod "Not Water" refers to any class other than high-confidence surface water (class 1). Similarly, "JRC Not Water" refers to JRC classes 0 and 1, while "JRC Water" refers to class 2 (Pekel et al., 2016).

imagery coincided with extensive flooding along the Mississippi River (USGS, 2020). DSWEmod imagery detected these inundation dynamics as well as those along the primary river channel (Figure 2a). Permanent channels with a width of 500–1,500 m (Figure 2a) and large water bodies (Figure 2b) were identified as water consistently throughout the year (i.e., up to 12 months); winter season snow and ice reduced the number of months that some lake pixels were classified as water. In contrast, DSWEmod did not consistently identify water within a narrower channel (250–750 m wide), where areas <500 m wide were not consistently identified as surface water

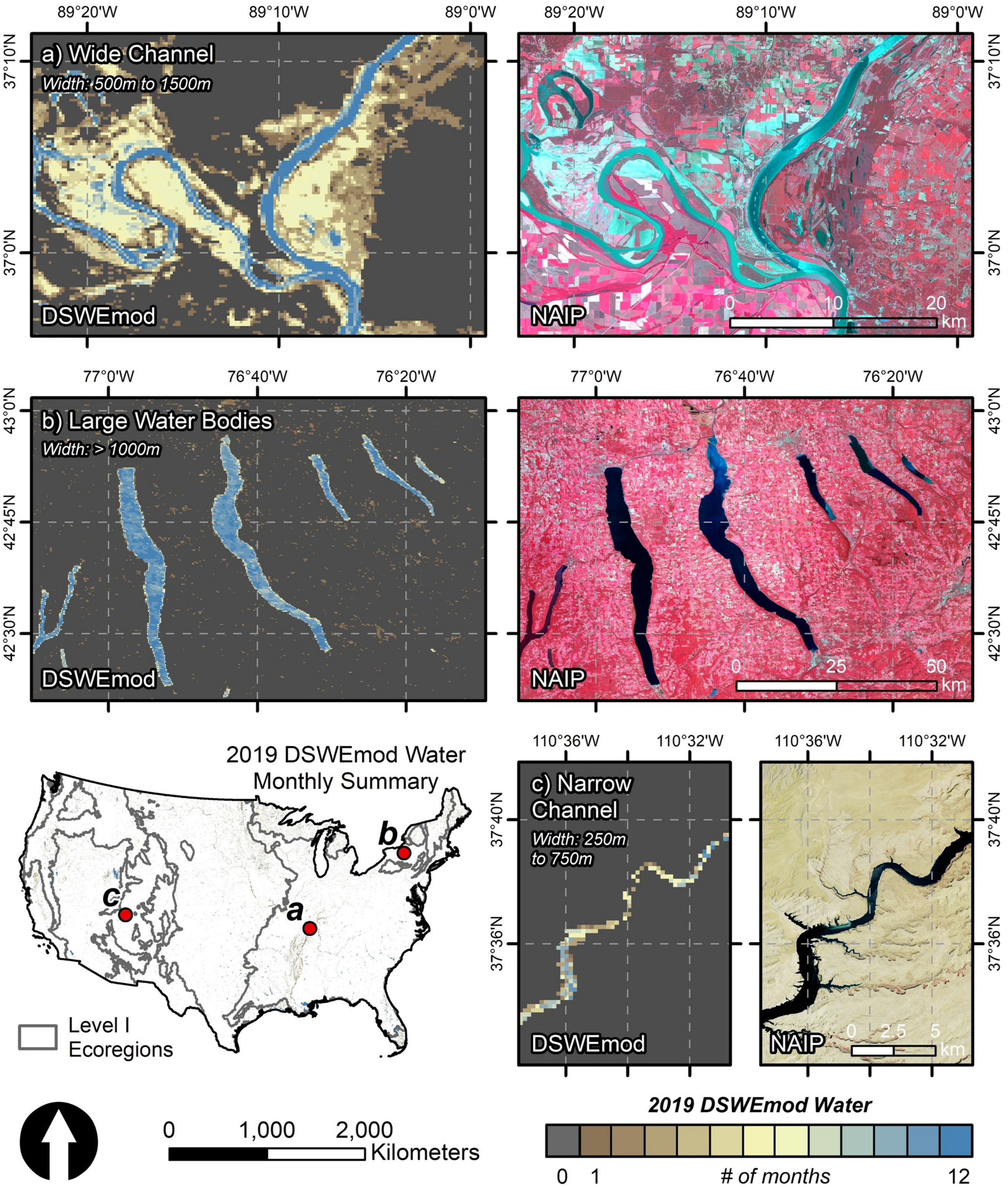

Figure 2. The spatial resolution capabilities of Dynamic Surface Water Extentmod (DSWEmod) water are demonstrated for three size classes of surface water objects. Monthly water presence/absence are summarized for 1 year (2019) in representative areas: (a) a wide channel (width: 500–1,500m), at the Mississippi-Ohio River confluence; (b) large water bodies (>25 ha; width: >1,000m), in the Finger Lakes of New York; and (c) a narrow channel (width: 250–750m), along the Colorado River arm of Lake Powell. To show detailed landscape conditions, each DSWEmod image is paired with false-color (NIR/red/green) NAIP imagery (USDA, 2021) (Source: Esri and the USDA Farm Service Agency; USA NAIP Imagery - Color Infrared).

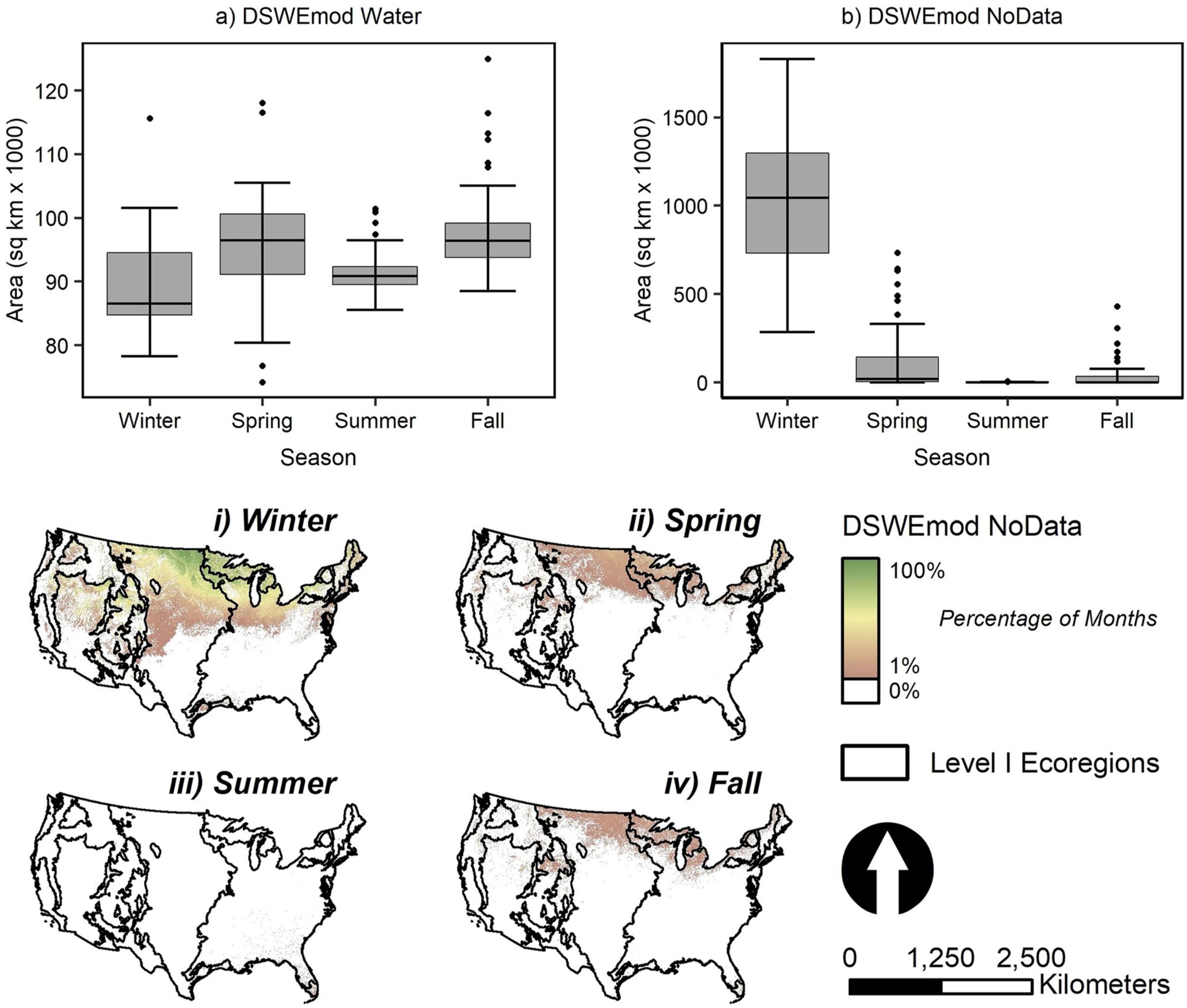

Figure 3. Seasonal distributions of surface water and NoData pixels in box plot and graphical form. Box plots (top) show (a) DSWEmod water and (b) DSWEmod NoData from 2003 through 2019 across the United States. Seasonal groups are winter, spring, summer, and fall. Note that *y*-axes are scaled individually. Maps (bottom; i–iv) show the seasonal distribution of DSWEmod NoData.

(Figure 2c). This inconsistency suggests that DSWEmod may identify surface water extent in larger channels and water bodies with relatively high certainty but may not necessarily identify pulses or consistent surface water flows within smaller stream/river networks or small water bodies.

3.1.3. Seasonal Variability in Water and NoData Pixels

DSWEmod water extents are seasonally variable for the US (Figure 3). The water extent mapped by DSWEmod is lowest (i.e., median value) during the winter months, followed by summer (Figure 3a). Mean surface water extents are similar in spring and fall, but most of the peaks in the DSWEmod time series occurred in the fall. The extent of clouds/cloud shadows and snow/ice (NoData) in DSWEmod is much higher in the winter compared to other seasons (Figure 3b; i–iv). The presence of snow, ice, clouds, and hillshade in the winter, spring, and fall seasons contributed to a reduction in mapped surface water in the northern and northeastern US, which also led to lower overall national estimates. At the national scale, DSWEmod NoData represents about 13% of each map for the winter months, compared to 0.01% during the summer months. The abundance of NoData during the winter season limits our ability to confidently identify water areas in select winter months in some parts of the country.

Table 2
Seasonal and Overall Surface Water Trends for Level I Ecoregions (Omernik, 1987) and the Conterminous United States Reported as Mann-Kendall Trend Values

Level I Ecoregion seasonal surface water trends

Level I Ecoregion	Winter	Spring	Summer	Fall	Overall
5 – Northern Forests	NA	−0.183	−0.417 *	−0.183	−0.142 *
6 – Northwestern Forested Mountains	0.015	−0.200	−0.133	−0.367	−0.077
7 – Marine West Coast Forest	0.029	0.029	−0.483 *	0.167	−0.048
8 – Eastern Temperate Forests	−0.086	0.367	0.103	−0.217	0.015
9 – Great Plains	NA	0.300	0.317	0.267	0.195 *
10 – North American Deserts	−0.124	−0.100	−0.150	0.059	0.006
11 – Mediterranean California	0	−0.267	0.033	−0.250	−0.021
12 – Southern Semi-Arid Highlands	0.147	−0.191	0.324	0.162	−0.008
13 – Temperate Sierras	−0.044	−0.221	0.183	0.412 *	0.001
15 – Tropical Wet Forests	0.567 *	−0.029	0.233	−0.132	0.009
Conterminous United States	0.236	0.183	0.100	0	0.040

Note. Positive and negative trends show increasing and decreasing surface water extents, respectively. Significance is indicated with * ($p < 0.05$). "NA" indicates fewer than 10 observations.

3.2. Level I Ecoregion Macro-Analysis

3.2.1. Seasonal and Overall Surface Water Trends

The results of the M-K tests show that surface water trends vary considerably across all time scales both within and between Level I Ecoregions (Table 2). For example, no ecoregions have consistent trends (negative or positive) overall and in all four seasons. The Northern Forests show negative trends, and the Great Plains show positive trends for all seasons except winter, which had too few values to support the application of the M-K test. The US also has positive trends overall and for all seasons other than the fall, which had no trend. The Marine West Coast Forest, on the other hand, has positive trends for the winter, spring, and fall, yet has a significant negative trend during the summer. Overall, only 6 of the 55 Level I Ecoregion trends (10.9%) were significant ($p < 0.05$).

3.2.2. Overview Statistics

An analysis of 204 monthly surface water maps (Petrakis et al., 2021) summarized by Level I Ecoregion provides general insights into spatiotemporal surface water dynamics from 2003 through 2019, including where water was most abundant or variable over the study period (Table 3). These results are consistent with known water cycle dynamics in these areas. For example, the Tropical Wet Forest Ecoregion in southern Florida represents the wettest part of the US, based on the largest proportion of surface water relative to the ecoregion extent. On average, water composed 10.3% of the ecoregion but episodically approached 20%. Surface water extents in larger ecoregions like the Great Plains and Eastern Temperate Forests cover proportionally smaller areas (i.e., proportion of 18,495 km^2 [0.8%] and 44,107 km^2 [1.7%], respectively). In most ecoregions, the water footprints typically undergo a 2-3× increase between the minimum and maximum values, but regions like the Northern Forests exhibit a ∼5.4× change between the minimum and maximum values while the US exhibits a slightly lower overall change (∼1.7×).

3.3. Level III Ecoregion Micro-Analysis

3.3.1. Mann-Kendall Trends

The Level III Ecoregion trends display more consistency across seasonal tests than the Level I Ecoregion analysis described in Section 3.2.1. Given the number and heterogeneity of the 85 Level III Ecoregions, we discuss only the most pronounced results of the trend analysis at this scale (Figure 4). Level III Ecoregions in the southwestern US, including the Sonoran Basin and Range (Level III Ecoregion #81), Mojave Basin and Range (#14), and Southern California/Northern Baja Coast (#85), exhibit the most consistent decreasing surface water trends

Table 3
General Statistics for Level I Ecoregions (Omernik, 1987) and the Conterminous United States

Level I Ecoregion surface water summary statistics

Level I Ecoregion	Mean surface water extent (km^2)	Minimum (km^2)	Maximum (km^2)	SD (km^2)	COV	Percent of ecoregion area (%)	Sen's monthly slope (km^2/month)
5 – Northern Forests	11,441.1	4,706.8	25,413.0	2,251.4	0.20	3.1	−2.3
6 – Northwestern Forested Mountains	5,397.8	2,596.8	7,217.4	805.7	0.15	0.6	−1.6
7 – Marine West Coast Forest	766.9	335.2	1,236.5	131.2	0.17	0.9	−0.1
8 – Eastern Temperate Forests	44,107.3	37,842.3	62,398.0	4,331.5	0.10	1.7	2.5
9 – Great Plains	18,494.6	12,513.1	28,210.1	2,344.7	0.13	0.8	10.4
10 – North American Deserts	11,402.8	9,425.2	14,336.7	996.3	0.09	0.8	0.3
11 – Mediterranean California	2,391.6	1,251.6	5,474.2	879.8	0.37	1.5	−0.5
12 – Southern Semi-Arid Highlands	7.7	0.5	45.8	8.0	1.04	0	−0.001
13 – Temperate Sierras	75.4	18.1	194.7	35.1	0.47	0.1	0.001
15 – Tropical Wet Forests	2,322.0	1,591.6	4,495.9	484.4	0.21	10.3	0.2
Conterminous United States	94,698.3	74,170.1	124,963.8	7,567.6	0.08	1.2	7.9

Note. Mean, standard deviation (SD), and coefficient of variation (COV) are based on annual surface water area from 2003 through 2019. Percent of ecoregion area is based on mean surface water extent relative to total area. The Sen's monthly slope references the Sen's slope quantified using all monthly surface water area values.

across the study period (Figure 4-i). In contrast, those in the central US (Figure 4-ii) have increasing surface water trends overall and across the seasonal time periods, consistent with the trends of the encompassing Great Plains Level I Ecoregion. The Northwestern Great Plains (#43), Nebraska Sand Hills (#44), and High Plains (#25) are in this group.

Some Level III Ecoregions exhibit pronounced trends in only one season. In the upper Midwest region surrounding the western Great Lakes (Figure 4-iii) several ecoregions have significant decreasing trends during the summer but non-significant trends during the other seasons. These ecoregions, which are characterized by high amounts of permanent surface water, include the Northern Lakes and Forests (#50), Northern Minnesota Wetlands (#49), and North Central Hardwood Forests (#51), and Lake Agassiz Plain (#48). These significant trends are also documented across the overall time series. Similarly, the Mississippi Alluvial Plain (#73) along the lower floodplain of the Mississippi River basin (Figure 4-iv), has a significant increasing trend in the spring, as do the Ouachita Mountains (#36) and South Central Plains (#35). Along the Gulf of Mexico, the Western Gulf Coastal Plain (#34) also has a significant increasing trend in only one season – the summer – with a non-significant decreasing trend in the fall.

Spatial complexity within Level I Ecoregions is apparent in the Eastern Temperate Forests ecoregion, where Level III Ecoregions in the eastern portion have seasonally conditioned decreasing surface water trends (Figure 4-v), while those in the western portion generally have increasing, though largely non-significant, trends (Figure 4-iv).

3.3.2. Sen's Slope

Two broad and geographically distinct patterns of surface water slope are present across the US: (a) increasing slopes within the central section (including the Great Plains) and (b) decreasing slopes across the eastern and western sections (Figure 5). Though the directionality of monthly Sen's trend slope (hereafter slope) matches the overall M-K trends (Figure 4e), the magnitude of change varies. Within the central section, the highest slope for Level III Ecoregions is in the Northwestern Great Plains (#43; slope = 6.8 km^2/month). The Northwestern Glaciated Plains (#42; 1.85 km^2/month), Mississippi Alluvial Plain (#73; 1.64 km^2/month), and Southern Coastal Plain (#75; 1.55 km^2/month) followed, though with considerably lower slopes. This pattern of increasing slopes exists primarily within the Great Plains Level I Ecoregion, but also extends to the western portion of the Eastern Temperate Forests, and along the Atlantic coast.

Much of the eastern, upper Midwest, and northeastern regions of the US largely underwent a decline in surface water. The Great Lakes region had three of the strongest negative slopes, specifically the Northern Lakes and Forests (#50; −1.95 km^2/month), Lake Agassiz Plain (#48; −1.63 km^2/month), and North Central Hardwood

10.1029/2021WR031399

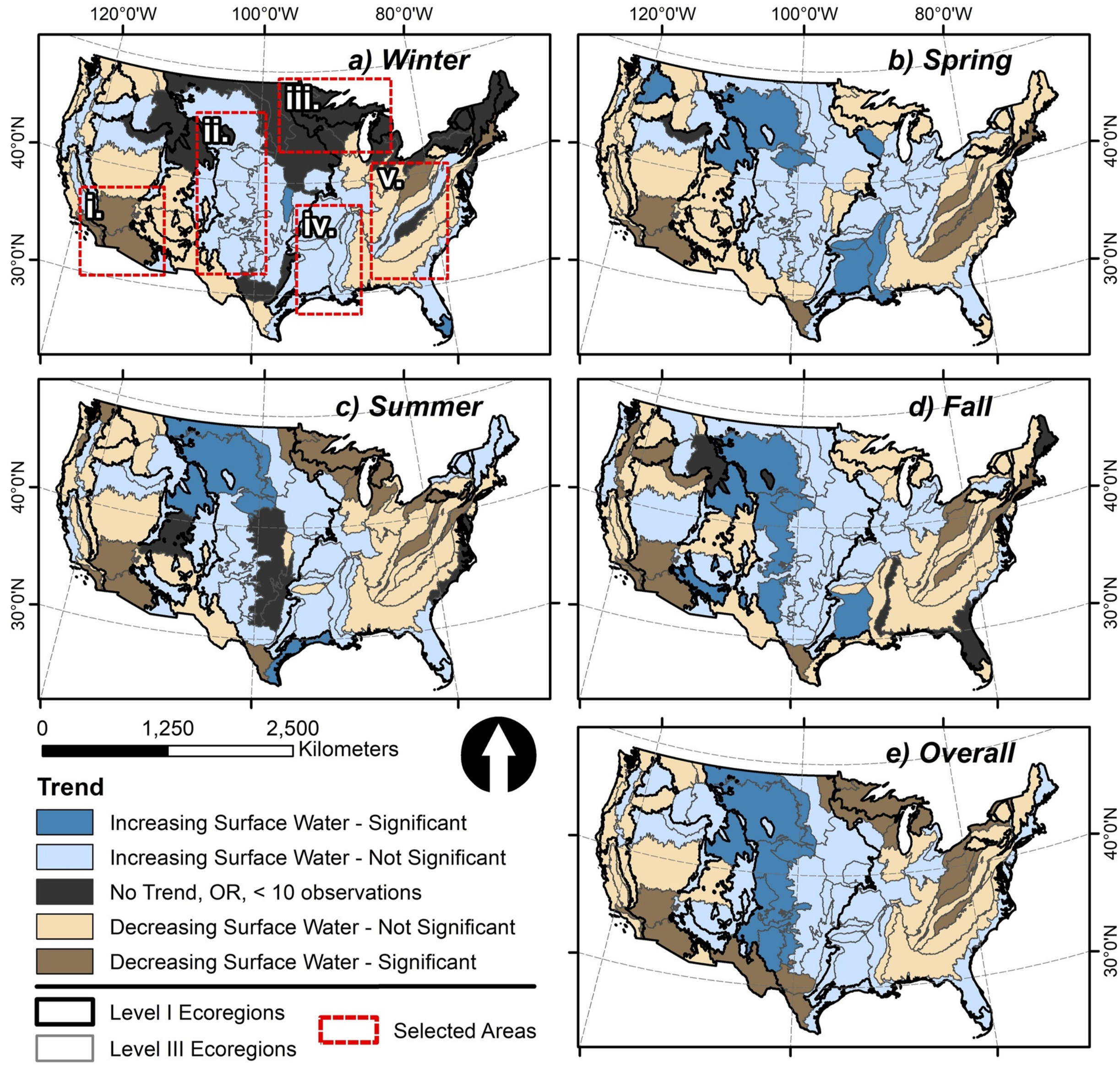

Figure 4. Seasonal and overall surface water trends in Level III Ecoregions (Omernik, 1987). Locations cited in the text (i–v) are outlined in the winter map (a).

Forests (#51; -1.1 km^2/month). Regions in the western US also underwent a widespread decline in surface water, with the most pronounced decreases observed in the Southwest. Some geographic variability is present across two Level I Ecoregions in the West: the Northwestern Forested Mountains and North American Deserts. In the North American Deserts, Level III Ecoregions with increasing slopes are generally found across the northern portions while decreasing slopes are present in the southern portions. The most extreme decreases occur in the Central (#13; -1.44 km^2/month), Mojave (#14; -0.62 km^2/month), and Sonoran (#81; -0.6 km^2/month) Basin and Range Ecoregions, though the Arizona/New Mexico Plateau (#22; 0.01 km^2/month) has a slight increasing slope. In the Northwestern Forested Mountains, Level III Ecoregions in the northwestern portions generally have decreasing surface water slopes while those across the southern and eastern portions have increasing slopes. The Temperate Sierras Level I Ecoregion, which only consists of one Level III Ecoregion, has a very low increasing slope (<0.01 km^2/month).

3.3.3. Streamgage Discharge and Surface Water Trend Congruency

Monthly M-K trends for DSWEmod surface water records (i.e., the overall trend) and discharge records were compared. As previously noted, a majority rule was applied to summarize the most common discharge trend

10.1029/2021WR031399

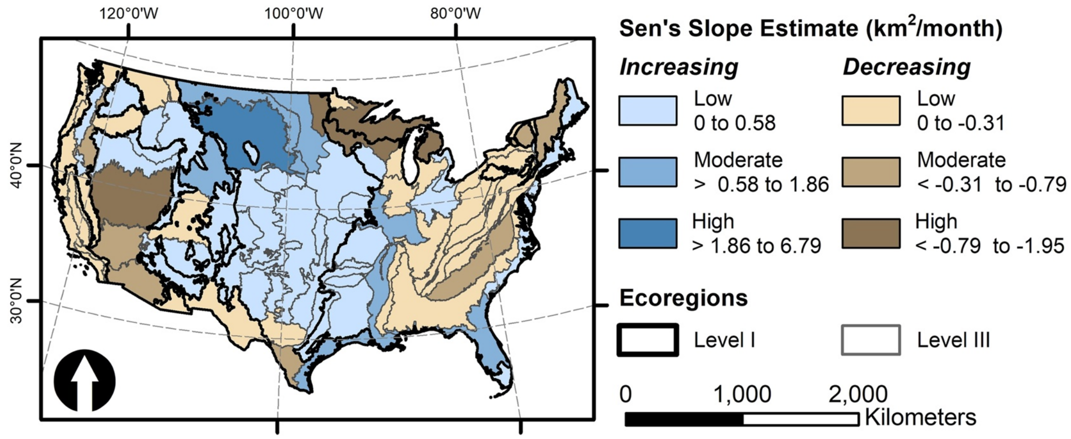

Figure 5. Sen's trend slope estimates (km^2/month) for DSWEmod-derived surface water extents in all Level III Ecoregions (Omernik, 1987). The estimates were grouped into the levels of increasing and decreasing slopes: (i) low, (ii) moderate, and (iii) high. Thresholds were manually assigned based on divisions in the data.

direction in each ecoregion over the study period. Results indicate a total of 54 (63.5%) Level III Ecoregions exhibited either positive (30 Level III Ecoregions) or negative (24 Level III Ecoregions) congruency between discharge and DSWEmod trends (Figure 6d). Of the 4,804 qualifying gages used in the national analysis, 59.1% (n = 2,840) had a trend direction matching that of the ecoregion that they were located within (Table 4). The Temperate Sierras (n = 1 Level III Ecoregion), Mediterranean California (n = 4), Great Plains (n = 16), and Northwestern Forested Mountains (n = 12) Level I Ecoregions include the most Level III Ecoregions with the same observed trend direction in both tests, with 100%, 100%, 87.5%, and 75% of ecoregions, respectively.

The remaining 30 Level III Ecoregions in the US demonstrate incongruency between discharge trends and surface water trends. Most of these ecoregions were located across the Great Lakes region, the southeastern US, and portions of the Basin and Range and Pacific Northwest regions of the western US (Figure 6d). In most cases (67%), incongruence was characterized by positive streamgage discharge trends and negative DSWEmod trends. These ecoregions include 3 (of 3 remaining) Northern Forests ecoregions, 11 (of 15 remaining) Eastern Temperate Forests ecoregions, and 2 (of 2 remaining) Marine West Coast Forest ecoregions. A cluster of ecoregions in the Southwest also exhibit poor correspondence, including the Central (#13) and Mojave (#14) Basin and Range Level III Ecoregions of the North American Deserts, and the Madrean Archipelago (#79) Level III Ecoregion.

4. Discussion

4.1. DSWEmod as a Source of Time-Series Data for Tracking Water Dynamics

Our assessment of the utility of DSWEmod surface water maps for monitoring water dynamics included considerations of innate MODIS data properties (i.e., sensor characteristics, masking accuracy, and viewing geometry) as well as a determination of how to effectively apply monthly surface water map composites compiled from daily MODIS images to describe multi-decadal trends for a large collection of ecoregions that make up the conterminous US.

Extending the regional methods applied to California (Soulard et al., 2022) to a national scale analysis highlights the complexity of tracking hydrologic change with MODIS data given moderate spatial resolution, viewing geometry challenges, and the presence of seasonal ice and snow in many parts of the US (Pickens et al., 2022). Despite these issues, the accuracy assessment of the DSWEmod data returned moderately high overall values for most Level I Ecoregions, with a few anomalies, including the Southern Semi-Arid Highlands ecoregion where reference data were sparse due to a paucity of sizable water bodies. Overall results were consistent with previously identified spatial and classification limits, such as the inability to accurately map pixels around water edges or smaller water bodies (Soulard et al., 2022). Effects related to the spatial variability of smaller water bodies on surface water trends vary by ecoregion, and since smaller, shallow water bodies are typically more responsive to transient weather events (i.e., floods or droughts), the absence of such features from our analysis likely limited

10.1029/2021WR031399

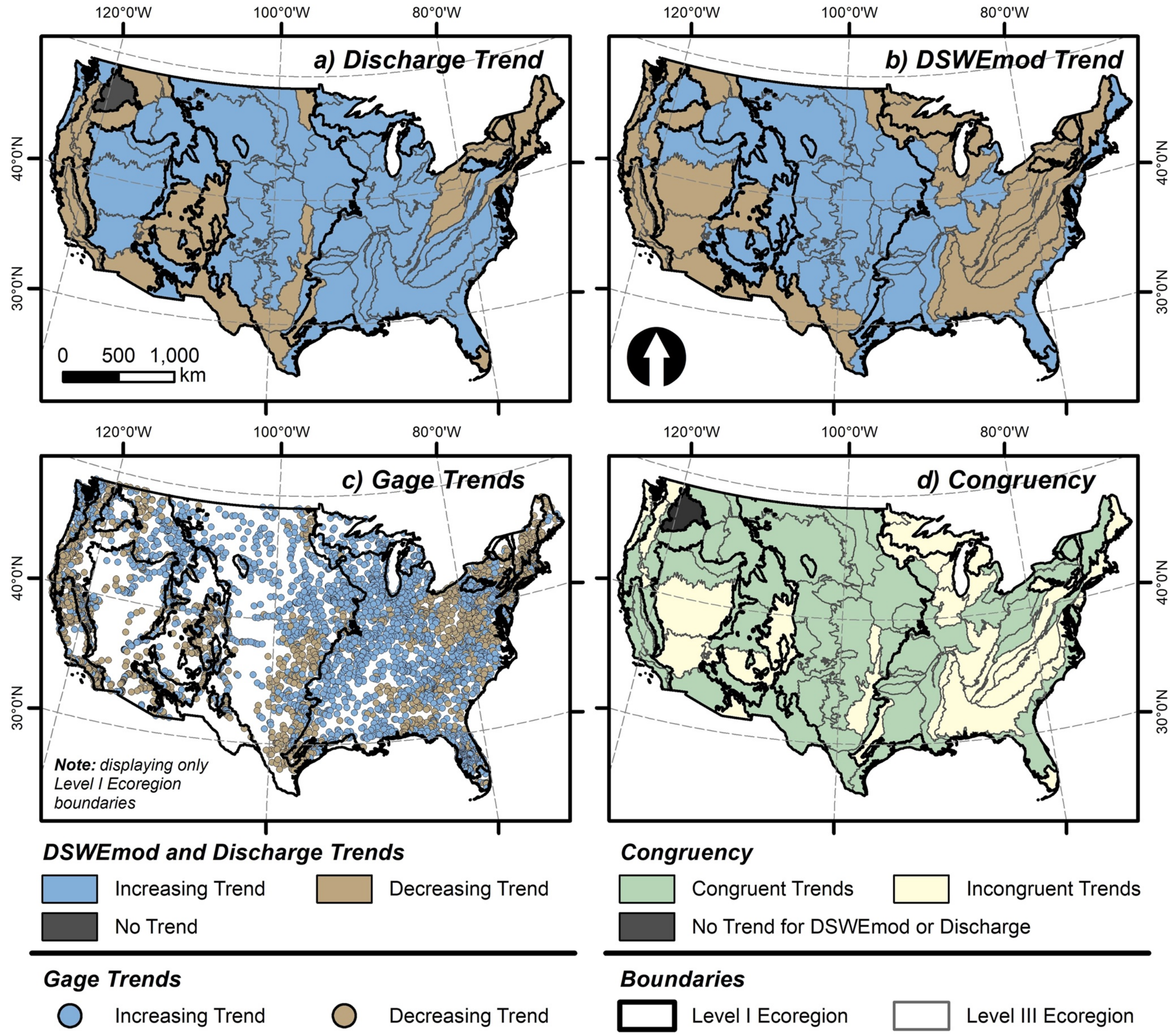

Figure 6. Overview of 2003–2019 trends in streamgage discharge and surface water extent across the United States. Trends are calculated for Level III Ecoregions (Omernik, 1987) according to (a) the majority of trends for all analyzed gages within each ecoregion (increasing/decreasing) across the monthly discharge records and (b) monthly records of DSWEmod surface water. In (c), the location and trend for each included gage illustrate the variability that can exist within ecoregions. The congruency map (d) highlights the geographical regions in which monthly gage discharge trends and DSWEmod surface water trends align.

variance and facilitated the identification of long-term surface water trends (Carroll & Loboda, 2017). An alternative source like Landsat imagery provides a higher spatial resolution capable of mapping smaller features, but MODIS provides a lengthy, continuous data record required for robust trend analysis (i.e., Mann-Kendall). While the surface water trends presented in this study primarily reflect only the dynamics of larger water bodies, such as lakes, reservoirs, and major rivers, MODIS remains the best available satellite resource for understanding contemporary annual and seasonal trends in surface water extent.

A second issue pertaining to the use of MODIS imagery as the foundation of this application is sensor degradation. Although prior (Collection 5) MODIS performance drift was addressed with radiometric calibration adjustments in the Collection 6 product, we observed remaining problems such as the increased frequency of negative values and decreased visible reflectance values over time for the shorter wavelengths of Terra imagery. These effects have been independently reported in the literature (e.g., Geng et al., 2019; Xiong et al., 2020, 2019; Zhang

Table 4

General Statistics for Each Level I Ecoregion (Omernik, 1987) and the Conterminous United States Summarizing DSWEmod Surface Water and Streamgage Discharge Trend Congruency Among Respective Level III Ecoregions

Level I Ecoregion trend congruency summary				
Level I Ecoregion	Count of Level III Ecoregions	Percent of Level III Ecoregions with congruent trends (%)	Number of gages tested	Percent of gages with congruent Trend (%)
5 – Northern Forests	4	25	200	49.5
6 – Northwestern Forested Mountains	12	75	675	61.5
7 – Marine West Coast Forest	3	33.3	131	41.2
8 – Eastern Temperate Forests	33	54.5	2189	52.8
9 – Great Plains	16	87.5	804	73.4
10 – North American Deserts	10	60	504	60.9
11 – Mediterranean California	4	100	244	78.7
12 – Southern Semi-Arid Highlands	1	0	12	41.7
13 – Temperate Sierras	1	100	30	56.7
15 – Tropical Wet Forests	1	0	15	40
Conterminous United States	85	63.5	4804	59.1

Note. Percentage of gages with congruent trends refers to gages that had congruent trends with the surface water trend of the Level III Ecoregion.

et al., 2017). Our observations of increasing frequency of negative reflectance values for water bodies correspond with increased flagging of "high aerosol" levels and general declines in visible reflectance near and over inland water. Despite the performance degradation, which can be considered an inevitable decline in instrument functionality given that the MODIS sensors are operating far beyond the designed 6-year lifespan (Lyapustin et al., 2014), the sensors continue to meet predetermined quality standards (Xiong et al., 2020).

Our internal qualitative and quantitative checks suggest that the issues above do not appear to occur abundantly enough to make a noticeable impact on map accuracy and trend determination for most of the US, but we did observe slightly higher error frequency in certain locations, giving us concern about sensor degradation. We posit that less-optimal mapping performance in the East, the Southwest, and within the Southern Semi-Arid Highlands Level I Ecoregion, where a combination of sensor degradation and cloud shadow effects, such as during the summer monsoon season, may have resulted in increasing errors of commission throughout the study period. We describe possible future image processing improvements in Section 4.4. An additional consideration of DSWEmod utility in this study was the determination of how well daily optical data could be leveraged for trend detection across the US. We summarized cloud, snow, and ice obstruction over the DSWEmod time series to assess the benefits of daily acquisitions compared to less frequent observations. Our analysis succeeded in mapping water features with MODIS across all seasons, but certain seasonal effects persisted. For example, the winter months (December – February) had overall higher proportions of obscured pixels over much of the US due to increased cloud and snow/ice cover, as well as lower sun angles which result in higher numbers of terrain-shaded (i.e., masked) pixels in the DSWE algorithm; widespread NoData values were also present in the spring and fall seasons – typically limited to March (spring) and November (fall) – across portions of the northern and northeastern US. These issues led to poor data quality over part of the time series and constrained subsequent trend analysis to spring, summer, and fall in those areas. While our MODIS approach overcomes cloud, snow, and ice obstruction issues across the US for most of the year, these results highlight the difficulty in assembling clear, high-frequency views of the landscape with optical satellite data, even with the availability of daily acquisitions.

4.2. Trends in Surface Water Patterns

The intent of our trend analysis was to distinguish monotonic trends in surface water extents over the 17-year time frame of this study. At a broad geographical scale (Level I Ecoregions), our results show that much of the western and eastern US has undergone a decline in surface water, while the Great Plains generally have had positive trends. These findings are largely consistent with those from other studies of recent water dynamics (e.g., Zou et al., 2018).

A fundamental difficulty with detecting trends is that abrupt, irregular variations may obscure an existing trend or contribute to the erroneous determination of one (Frei & Schar, 2000). While M-K tests are robust to the influence of outliers, short-term dynamics on overall trends are relevant in places like the lower Mississippi River basin, which had extensive floods in April and May of 2008, 2011, 2016, 2018, and 2019 (National Weather Service, 2019). Our tests found a significantly increasing surface water trend in the spring for the Mississippi Alluvial Plain (#73) Level III Ecoregion (Figure 4) coinciding with large-scale inundation events in the latter half of the study period.

Given that the onset and duration of droughts are typically more gradual and extended than flooding events, decreasing time-series are less likely to be affected by the types of abrupt, stochastic variations that confound the detection of increasing trends (Shao & Kam, 2020). We observed significant decreasing overall and seasonal water trends for many Level III Ecoregions in the Southwest, an area undergoing a long-term (>100 years) drought (Figure 4) (Cayan et al., 2010; Cook et al., 2015; MacDonald et al., 2008; Seager et al., 2013). Similarly, we identified significant decreasing trends in several Level III Ecoregions in the Southeast, as well as within the western Great Lakes region during the summer. Specifically, summer surface water coverage decreased at a rate of 1.95 km^2/month in the Northern Lakes and Forests Level III Ecoregion (#50).

Continued surface water monitoring may identify changes in these trends in the future. For example, long-term climate projections across the Midwest suggest earlier surface water flows in the spring, coupled with increased temperature and decreased precipitation during the summer, which may reduce stream flow and surface water locally (Byun et al., 2019; Byun & Hamlet, 2018). Additionally, Topp et al. (2021) identified ongoing transitions in the seasonality of algal blooms across portions of the Midwest, where the phenology pattern is shifting at some locations from spring to summer presence. Changes in the concentrations of nutrient enrichment in the water (Carpenter & Pace, 2018) would theoretically result in reductions in the classification of DSWEmod water during certain seasons as a result of mixed vegetation/water pixels and may be partially driving a decreasing summer trend.

General surface water metrics (i.e., minimum, maximum, mean, coefficient of variation) of each regional time series may also supplement trend analyses by helping illustrate both inter-annual effects (e.g., climate variability) and seasonal effects (e.g., seasonal variability of precipitation and evaporation). For example, minimum and maximum water extents in the Northern Forests (which includes parts of Minnesota, Wisconsin, Michigan, Massachusetts, Pennsylvania, and New York) represent the seasonal alternation between frozen winter conditions and peak summer water area (Pickens et al., 2022), while in Mediterranean California they represent summer drought and rainy winter conditions. Applying 204 monthly observations derived for each ecoregion in the US to analyze annual trends, seasonal trends, and punctuated changes within the time series provides a great opportunity to explore the role of seasonal weather (i.e., precipitation, evapotranspiration, the timing of snow and snowmelt), climate trends, biophysical and hydrological characteristics, and human drivers (i.e., demand, purveyance, etc.) on regional surface water in the 21st century. The core analyses included in this application do not focus on quantifying the sensitivity of water bodies to regional drivers yet represent a starting point for using satellite imagery to chronicle the rates and trends of surface water change in the US that can feed into a more robust analysis of cause and effect.

4.3. Streamgage Discharge and Surface Water Congruency

The use of continuous DSWEmod monthly composites to calculate seasonal and overall trends for every Level III Ecoregion represents a new way of quantifying surface water dynamics in the US. It is logical to compare these trends to other established approaches to identify where similarities and differences exist. One of the most commonly used hydrologic observation tools in the US is the USGS streamgage network, which includes over 10,000 active gages with thousands more that measured data at some point during our study period (USGS NWIS, 2022d). To compare datasets, we calculated discharge trends across all available qualifying gages to create a synoptic view of flow for each ecoregion. We then compared discharge trend direction (i.e., increasing or decreasing) to surface water trend direction to identify regions where the drivers that affect flow may also have a similar influence on water area, as well as areas where trend direction differed over the study period. We defined congruency to exist when the majority of streamgage discharge trends in a given ecoregion show similar directionality as the DSWEmod-derived surface water trend in the same ecoregion. Using this approach, we determined that most (e.g., 63.5%) ecoregions had congruent trends. On a more granular level, nearly 60% of the individual gages used in this analysis exhibited the same trend direction as DSWEmod for the ecoregions in which they were located. Patterns of congruency differed according to trend direction. Thirty of the 41 Level III Ecoregions (73.2%) with positive overall DSWEmod trends also had positive discharge trends. Similarly, over 80% ($n = 1{,}325$ of 1,647) of the gages tested within these ecoregions had increasing discharge. There was slightly less congruency for decreasing trends. We found that 24 of 44 Level III Ecoregions (54.5%) with decreasing DSWEmod trends also had decreasing discharge trends. At the gage level, over 70% of the streamgages within these 24 ecoregions had decreasing trends. Collectively, these results indicate that surface water trends captured by DSWEmod align with streamgage trends across a large portion of the US.

Increasing trends were quantified for both surface water and discharge across the Great Plains and middle Rocky Mountain highlands. The areal extents of the water bodies that run through the Great Plains (e.g., Missouri River) are controlled by precipitation that is coincident with late-season snowmelt originating from the Rocky Mountains (Quiring & Kluver, 2009), potentially driving coinciding changes in both discharge and surface water area. For the western uplands of the US, south Texas, and much of California, both DSWEmod and discharge had decreasing trends, suggesting similar surface water and discharge dynamics in this region as well. While the 63.5% of ecoregions with congruent trends may indicate that both streamflow and surface water dynamics are largely responding to the same drivers, we also acknowledge that congruency may arise from independent drivers that coincidentally result in similar trends. However, in the absence of benchmark studies of nationwide surface water trends that would allow for more definitive confirmation, positive results in a given ecoregion allow a measure of confidence that the DSWEmod time series may be a reasonable proxy for gage-based measurements.

Conflicting trend directions, on the other hand, may reflect that, (a) external influences render either DSWEmod or discharge time series less appropriate for assessing surface water dynamics, (b) the drivers that influence each dataset may not be aligned, or (c) the two modes of measuring water change may be capturing different characteristics of water (i.e., flashier discharge on smaller streams vs. large water body dynamics). Discharge trend direction and surface water trend direction did not match for the remaining 31 Level III Ecoregions. Incongruent trends are found regionally across the Great Lakes, the Southeast, and portions of the West. In many of these cases of dissimilar trends, decreasing surface water is paired with increasing streamflow. One potential explanation for the lack of consistency has been discussed previously; namely, that detecting surface water trends with MODIS data may be hindered by either atmospheric effects or sensor-specific considerations such as look angle and instrument degradation. The DSWEmod imagery time series might thus be an incomplete record of true surface water dynamics in these areas. For instance, portions of the Great Lakes have experienced increases in extreme precipitation frequency (Paxton et al., 2021). Short-term periods of maximum discharge of surface water following extreme precipitation events may be missed using optical remote sensing datasets if there is extended cloudiness (Huang et al., 2018).

Another plausible explanation for mismatched streamgage and DSWEmod trends is that their dynamics may be driven by decoupled, independent factors that yield divergent results. For instance, variations in the management of water resources and climate stresses can impact water storage and surface flows differently. Across both the Central and Mojave Basin and Range Level III Ecoregions, water levels for many primary water bodies including Lake Mead (NASA, 2021), Mono Lake (Mono Basin Clearinghouse, 2021), Walker Lake (USGS NWIS, 2022b), Pyramid Lake (USGS NWIS, 2022c), and the Great Salt Lake, which can undergo significant reductions in the surface area following a minimal drop in water surface elevation (USGS NWIS, 2022a; Utah Water Science Center, 2021), have experienced regular declines in water level over the study period. These declines have occurred despite reductions in the total percentage of urban water use in large regional cities (i.e., Los Angeles, Phoenix, Las Vegas) during the 21st century (Richter et al., 2020), coupled with reductions in the amount of irrigated water use in southwestern states (though not including California) as a result of improvements in technology and management practices (Mpanga & Idowu, 2021). However, increasing discharge trends at some gages have been observed along the Jordan River upstream of the Great Salt Lake (USGS gage 10171000; M-K trend = 0.039), the Truckee River upstream of Pyramid Lake (10351700; 0.018), and the Walker River upstream of Walker Lake (10301600; 0.014) over the same period. A similar pattern may be present across portions of the Southeast, which has had documented decreases in water quantity, groundwater, and low-flow streamgage records (Engström et al., 2021; Richey et al., 2015; Stephens & Bledsoe, 2020), matching the decreasing trends seen in the DSWEmod time series, though in contrast to a majority of trends in discharge. Unlike the extended droughts that encompass the Southwest, this region experiences a greater frequency of short-term "flash droughts" and extreme wet events impacting both surface and groundwater flows (Engström et al., 2021; Labosier & Quiring, 2013).

Spatial biases may have also influenced the outcome of the trend analysis. HUCs are spatially disconnected from ecoregions, and discharge within an overlapping HUC may not always represent surface water conditions occurring within the respective ecoregion. As an example, gage trends across the Southeast (Figure 6c) suggest that this region may be more susceptible to spatial variability in trend direction that is not displayed at an ecoregion scale. The spatial distribution of streamgages is another source of potential discordance. Since streamgages cannot feasibly be installed on every waterway, the priority is to place them in locations that better inform human water management needs (Krabbenhoft et al., 2022), which inherently leads to spatiotemporal gaps in parts of the US. Spatial and temporal gaps are more common across portions of the central and western HUCs of the US, where lower correlations are present between gaged and ungaged locations and the ability to estimate flows at ungaged locations is limited (Kiang et al., 2013). This point-based sampling differs from the comprehensive DSWEmod product, which provides wall-to-wall measurements of surface water dynamics. Our decision to retain streamgages with discharge above the bottom quartile threshold also biased the analysis toward larger order waterways. While both factors may make the comparison approach slightly less suitable in parts of the country with spatiotemporal gaps, we feel that the selection criteria allow us to create a more equitable comparison with the moderately sized water bodies that we mapped with MODIS.

We do not explore the full range of reasons for congruent or incongruent trends between the two measurement approaches since an in-depth review of the individual drivers in every ecoregion is beyond the scope of this paper. However, describing the relationship between instrumented surface water flows and DSWEmod across various landscapes may be helpful for water management applications inside the US, while also justifying the use of satellite imagery as a proxy for trends derived from in-situ measurements in parts of the US where the landscape is not consistently covered by clouds, snow, or ice.

4.4. Future Directions and Applications

There are ample possibilities for reducing errors in MODIS-derived maps and employing different analytical approaches to glean additional insights into the causes and patterns of surface water change. Improvements in the preprocessing of MODIS data will provide future opportunities to verify the existence and magnitude of any subtle trends detected here. The Multi-Angle Implementation of Atmospheric Correction (MAIAC) algorithm is a sophisticated method for cloud detection, aerosol retrieval, and atmospheric corrections; its application to Collection 6 data has improved the accuracy of measured surface reflectance values to the extent that MAIAC data are now the standard dataset for MODIS-based studies of land-surface dynamics (Lyapustin et al., 2018). We intend to generate updated DSWEmod layers with MAIAC data once they are available through the GEE public catalog.

Additionally, we can apply a variety of approaches in future analyses to better understand the causes and patterns of surface water dynamics and change. A multi-variate approach could quantify simultaneous drivers, while the removal of managed water bodies, which are more strongly influenced by water management than weather (Fergus et al., 2020), may help to isolate climate responses. For more static water bodies such as lakes and reservoirs, which DSWEmod is more adept at identifying due to pixel size limitations, lagged drivers are shown to be valuable in driving surface water extent dynamics (Heimhuber et al., 2017) and may be worth considering in future analyses. Other changes in LULC can have underlying impacts on surface water dynamics, including changes in urban area (e.g., expansion and intensity), agricultural practices (e.g., irrigation, evapotranspiration), vegetation cover and type (e.g., water use), and could improve our understanding of regional drivers of surface water (Schilling et al., 2008; Stonestrom et al., 2009). These options may prove effective for quantifying how surface water extents change in response to human and natural factors across some of the ecoregions with more complex hydrologic dynamics. Finally, the national scale of the trend analysis and discharge comparison does not allow for the full exploration of the regional disconnect between different types of water metrics. Future research could focus on evaluating the role of common streamflow drivers (Slater & Villarini, 2017) on surface water trends to identify if similar statistical relationships extend between each time series.

5. Conclusions

Our research approach was effective in determining three main aspects of surface water dynamics across the US: (a) a general overview of surface water presence and yearly variability, (b) seasonal and overall trends of surface water summarized at the ecoregion scale, and (c) a test of the congruency between trends of streamgage discharge and surface water, also summarized by ecoregion. The results of this study have identified regional and localized trends in surface water extents and provide a basic overview of where and to what extent trends in surface water and discharge align over the past two decades.

This investigation represents an important step toward quantifying multi-temporal surface water trends based on monthly imagery data, setting the stage for future work that integrates localized human activities into more robust casual analyses. Comparing streamgage discharge and satellite-derived maps indicates that fluctuations in streamflow and surface water area are linked in most of the US; the trend direction in DSWEmod and streamgage records were congruent in more than 60% of US ecoregions. The positive surface water and discharge trends in the Great Plains over the study period reaffirm prior findings of an increase in surface water across the central and upper Midwest in recent decades (Gupta et al., 2015; Zou et al., 2018). In this study, surface water area across the Great Plains Level I Ecoregion increased at a rate (e.g., Sen's slope) of 124.8 km^2/year, leading to a substantial increase in surface water that may be, in part, due to an increase in regional precipitation over the same period of time (Thornton et al., 2020). Negative trends within selected Level III Ecoregions across the West include the Central Valley of California (−3.2 km^2/year), the Mojave Basin and Range (−7.5 km^2/year), and the Sonoran Basin and Range (−7.2 km^2/year), coinciding with discharge records in each ecoregion showing declines over the same period. While trends align in many parts of the US, our analysis does also find that parts of the country had poor correspondence between trends in DSWEmod and streamgage discharge, including sections of the Great Lakes and Southeast. By providing possible explanations for this without fully resolving underlying drivers, we lay out a roadmap for future applications focused on regional causal processes.

Assembling clear views of the landscape at a monthly timestep broadens opportunities to monitor intra- and inter-annual trends and identify differences between heterogeneous ecosystems. Understanding the underlying driving forces that contribute to these changes is far more challenging, but this work presents a template for future examinations that can incorporate a larger suite of possible explanatory variables and account for regional differences. While the linkage between streamflow and surface water area is not absolute across ecoregions, our comparison highlights how satellite records can complement streamgage measurements and help create a more complete understanding of water dynamics at the regional scale. Dissimilar trends suggest that it is premature to conclude that MODIS-based surface water maps can serve as a proxy for streamflow in all parts of the world, but these data can provide other valuable insights on long-term trends, especially in regions without long periods of snow or cloud cover.

Data Availability Statement

Data products for this research can be found on the U.S. Geological Survey ScienceBase public data repository (Petrakis et al., 2021).

Acknowledgments
Funding for this work was provided by the U.S. Geological Survey (USGS) Climate Research and Development Program of the Ecosystems Mission Area. Thank you to Britt Smith (USGS) for providing insight and assisting in the early reviews of the manuscript. Thank you to Melanie Vanderhoof (USGS) for providing a constructive review of the manuscript as well as to the anonymous journal reviewers. Any use of trade, firm, or product names is for descriptive purposes only and does not imply endorsement by the U.S. Government.

References

Austin, S. H., Wolock, D. M., & Nelms, D. L. (2017). *Variability of Hydrological Droughts in the conterminous United States, 1951 through 2014* (Scientific investigations Report No. 2017–5099). U.S. Geological Survey.

Bales, J. D., & Wagner, C. R. (2009). Sources of uncertainty in flood inundation maps. *Journal of Flood Risk Management*, *2*(2), 139–147. https://doi.org/10.1111/j.1753-318X.2009.01029.x

Banerjee, C., & Kumar, D. N. (2018). Assessment of Surface Water Storage trends for increasing groundwater areas in India. *Journal of Hydrology*, *562*, 780–788. https://doi.org/10.1016/j.jhydrol.2018.05.052

Bayazit, M., & Önöz, B. (2007). To prewhiten or not to prewhiten in trend analysis? *Hydrological Sciences Journal*, *52*(4), 611–624. https://doi.org/10.1623/hysj.52.4.611

Bronaugh, D., & Werner, A. (2013). R package zyp. R foundation for statistical computing. Retrieved from https://cran.r-project.org/web/packages/zyp/zyp.pdf

Bureau of Reclamation (2020). Bureau of Reclamation water operations. Retrieved from https://www.usbr.gov/main/water/

Byun, K., Chiu, C.-M., & Hamlet, A. F. (2019). Effects of 21st century climate change on seasonal flow regimes and hydrologic extremes over the Midwest and Great Lakes region of the US. *Science of The Total Environment*, *650*, 1261–1277. https://doi.org/10.1016/j.scitotenv.2018.09.063

Byun, K., & Hamlet, A. F. (2018). Projected changes in future climate over the Midwest and Great Lakes region using downscaled CMIP5 ensembles. *International Journal of Climatology*, *38*, e531–e553. https://doi.org/10.1002/joc.5388

Carpenter, S. R., & Pace, M. L. (2018). Synthesis of a 33-yr series of whole-lake experiments: Effects of nutrients, grazers, and precipitation-driven water color on chlorophyll. *Limnology and Oceanography Letters*, *3*(6), 419–427. https://doi.org/10.1002/lol2.10094

Carroll, M., & Loboda, T. (2017). Multi-decadal surface water dynamics in North American Tundra. *Remote Sensing*, *9*(5), 497. https://doi.org/10.3390/rs9050497

Cayan, D. R., Das, T., Pierce, D. W., Barnett, T. P., Tyree, M., & Gershunov, A. (2010). Future dryness in the Southwest US and the hydrology of the early 21st century drought. *Proceedings of the National Academy of Sciences*, *107*(50), 21271–21276. https://doi.org/10.1073/pnas.0912391107

Congalton, R. G. (1991). A review of assessing the accuracy of classifications of remotely sensed data. *Remote Sensing of Environment*, *37*, 35–46. https://doi.org/10.1016/0034-4257(91)90048-B

Cook, B. I., Ault, T. R., & Smerdon, J. E. (2015). Unprecedented 21st century drought risk in the American southwest and central Plains. *Science Advances*, *1*(1), e1400082. https://doi.org/10.1126/sciadv.1400082

DeCicco, L. A., & Hirsch, R. M. (2021). Introduction to the dataRetrieval package. Retrieved from https://cran.r-project.org/web/packages/dataRetrieval/vignettes/dataRetrieval.html

DeVries, B., Huang, C., Armston, J., Huang, W., Jones, J. W., & Lang, M. W. (2020). Rapid and robust monitoring of flood events using Sentinel-1 and Landsat data on the Google Earth Engine. *Remote Sensing of Environment*, *240*, 111664. https://doi.org/10.1016/j.rse.2020.111664

Dieter, C. A., Maupin, M. A., Caldwell, R. R., Harris, M. A., Ivahnenko, T. I., Lovelace, J. K., et al. (2017). *Estimated Use of Water in the United States in 2015* (USGS open-File Report No. 2017–1131). U.S. Geological Survey.

Downton, M. W., Miller, J. Z. B., & Pielke, R. A. (2005). Reanalysis of U.S. National Weather Service flood loss database. *Natural Hazards Review*, *6*(1), 13–22. https://doi.org/10.1061/(ASCE)1527-6988(2005)6:1(13)

Engström, J., Praskievicz, S., Bearden, B., & Moradkhani, H. (2021). Decreasing water resources in Southeastern U.S. as observed by the GRACE satellites. *Water Policy*, *23*(4), 1017–1029. https://doi.org/10.2166/wp.2021.039

Fergus, C. E., Brooks, J. R., Kaufmann, P. R., Herlihy, A. T., Pollard, A. I., Weber, M. H., & Paulsen, S. G. (2020). Lake water levels and associated hydrologic characteristics in the conterminous U.S. *JAWRA Journal of the American Water Resources Association*, *56*(3), 450–471. https://doi.org/10.1111/1752-1688.12817

Frei, C., & Schar, C. (2000). Detection probability of trends in rare events: Theory and application to heavy precipitation in the Alpine region. *Journal of Climate*, *14*, 17.

Garen, D. C. (1993). Revised surface-water supply index for Western United States. *Journal of Water Resources Planning and Management*, *119*(4), 437–454. https://doi.org/10.1061/(asce)0733-9496(1993)119:4(437)(1993)119:4(437

Geng, X., Li, Y., Twedt, K., & Xiong, X. (2019). Improvements in the on-orbit response versus scan-angle characterization for the MODIS ocean color bands. *Proceedings Sensors, Systems, and Next-Generation Satellites*, *XXIII*, 11151. https://doi.org/10.1117/12.2532081

Gorelick, N., Hancher, M., Dixon, M., Ilyushchenko, S., Thau, D., & Moore, R. (2017). Google Earth Engine: Planetary-scale geospatial analysis for everyone. *Remote Sensing of Environment*, *202*, 18–27. https://doi.org/10.1016/j.rse.2017.06.031

Griffith, G. E., Omernik, J. M., & Woods, A. J. (1999). Ecoregions, watersheds, basins, and HUCs: How state and federal agencies frame water quality. *Journal of Soil and Water Conservation*, *54*(4), 666–677.

Gupta, S. C., Kessler, A. C., Brown, M. K., & Zvomuya, F. (2015). Climate and agricultural land use change impacts on streamflow in the upper midwestern United States. *Water Resources Research*, *51*(7), 5301–5317. https://doi.org/10.1002/2015WR017323

Hamed, K. H. (2008). Trend detection in hydrologic data: The Mann–Kendall trend test under the scaling hypothesis. *Journal of Hydrology*, *349*(3–4), 350–363. https://doi.org/10.1016/j.jhydrol.2007.11.009

Heimhuber, V., Tulbure, M. G., & Broich, M. (2017). Modeling multidecadal surface water inundation dynamics and key drivers on large river basin scale using multiple time series of Earth-observation and river flow data. *Water Resources Research*, *53*(2), 1251–1269. https://doi.org/10.1002/2016WR019858

Huang, C., Chen, Y., Zhang, S., & Wu, J. (2018). Detecting, extracting, and monitoring surface water from space using optical sensors: A review. *Reviews of Geophysics*, *56*(2), 333–360. https://doi.org/10.1029/2018RG000598

Jin, S., & Sader, S. A. (2005). Comparison of time series tasseled cap wetness and the normalized difference moisture index in detecting forest disturbances. *Remote Sensing of Environment*, *94*(3), 364–372. https://doi.org/10.1016/j.rse.2004.10.012

Jones, J. (2015). Efficient wetland surface water detection and monitoring via Landsat: Comparison with in situ data from the Everglades depth estimation network. *Remote Sensing*, *7*(9), 12503–12538. https://doi.org/10.3390/rs70912503

Jones, J. (2019). Improved automated detection of subpixel-scale inundation—Revised Dynamic Surface Water Extent (DSWE) partial surface water tests. *Remote Sensing*, *11*(4), 374. https://doi.org/10.3390/rs11040374

Karl, T. R., & Riebsame, W. E. (1989). The impact of decadal fluctuations in mean precipitation and temperature on runoff: A sensitivity study over the United States. *Climatic Change*, *15*(3) , 423–447. https://doi.org/10.1007/BF00240466

Kendall, M. G. (1975). *Rank correlation methods*. Griffin.

Khandelwal, A., Karpatne, A., Marlier, M. E., Kim, J., Lettenmaier, D. P., & Kumar, V. (2017). An approach for global monitoring of surface water extent variations in reservoirs using MODIS data. *Remote Sensing of Environment*, *202*, 113–128. https://doi.org/10.1016/j.rse.2017.05.039

Kiang, J. E., Stewart, D. W., Archfield, S. A., Osborne, E. B., & Eng, K. (2013). (pp. 1–94). *A national streamflow network gap analysis* (Scientific investigations Report No. 2013–5013). *U.S. Geological Survey and U.S. Fish and Wildlife Service*. Retrieved from https://pubs.er.usgs.gov/publication/sir20135013

Krabbenhoft, C. A., Allen, G. H., Lin, P., Godsey, S. E., Allen, D. C., Burrows, R. M., et al. (2022). Assessing placement bias of the global river gauge network. *Nature Sustainability*. https://doi.org/10.1038/s41893-022-00873-0

Krueger, E. S., Yimam, Y. T., & Ochsner, T. E. (2017). Human factors were dominant drivers of record low streamflow to a surface water irrigation district in the US southern Great Plains. *Agricultural Water Management*, *185*, 93–104. https://doi.org/10.1016/j.agwat.2017.01.018

Kunkel, K. E., Andsager, K., & Easterling, D. R. (1999). Long-term trends in extreme precipitation events over the conterminous United States and Canada. *Journal of Climate*, *12*, 13. https://doi.org/10.1175/1520-0442(1999)012<2515:lttiep>2.0.co;2

Labosier, C., & Quiring, S. (2013). Hydroclimatology of the southeastern USA. *Climate Research*, *57*(2), 157–171. https://doi.org/10.3354/cr01166

Libiseller, C., & Grimvall, A. (2002). Performance of partial Mann-Kendall tests for trend detection in the presence of covariates. *Environmetrics*, *13*(1), 71–84. https://doi.org/10.1002/env.507

Lins, H. F., & Slack, J. R. (1999). Streamflow trends in the United States. *Geophysical Research Letters*, *26*(2), 227–230. https://doi.org/10.1029/1998GL900291

Lins, H. F., & Slack, J. R. (2005). Seasonal and regional characteristics of U.S. streamflow trends in the United States from 1940 to 1999. *Physical Geography*, *26*(6), 489–501. https://doi.org/10.2747/0272-3646.26.6.489

Lyapustin, A., Wang, Y., Korkin, S., & Huang, D. (2018). MODIS collection 6 MAIAC algorithm. *Atmospheric Measurement Techniques*, *11*, 5741–5765. https://doi.org/10.5194/amt-11-5741-2018

Lyapustin, A., Wang, Y., Xiong, X., Meister, G., Platnick, S., Levy, R., et al. (2014). Scientific impact of MODIS C5 calibration degradation and C6+ improvements. *Atmospheric Measurement Techniques*, *7*(12), 4353–4365. https://doi.org/10.5194/amt-7-4353-2014

MacDonald, G. M., Stahle, D. W., Diaz, J. V., Beer, N., Busby, S. J., Cerano-Paredes, J., et al. (2008). Climate warming and 21st-century drought in southwestern North America. *Eos, Transactions American Geophysical Union*, *89*(9), 82. https://doi.org/10.1029/2008EO090003

Mann, H. B. (1945). Nonparametric tests against trend. *Econometrica*, *13*(3), 245. https://doi.org/10.2307/1907187

Milano, M., Ruelland, D., Fernandez, S., Dezetter, A., Fabre, J., Servat, E., et al. (2013). Current state of Mediterranean water resources and future trends under climatic and anthropogenic changes. *Hydrological Sciences Journal*, *58*(3), 498–518. https://doi.org/10.1080/02626667.2013.774458

Miller, W. P., & Piechota, T. C. (2011). Trends in Western U.S. Snowpack and Related Upper Colorado River Basin Streamflow. *JAWRA Journal of the American Water Resources Association*, *47*(6), 1197–1210. https://doi.org/10.1111/j.1752-1688.2011.00565.x

Mono Basin Clearinghouse. (2021). *Mono Lake levels 1850-present* [Dataset]. https://www.monobasinresearch.org/data/levelyearly.php

Mpanga, I. K., & Idowu, O. J. (2021). A decade of irrigation water use trends in southwestern USA: The role of irrigation technology, best management practices, and outreach education programs. *Agricultural Water Management*, *243*, 106438. https://doi.org/10.1016/j.agwat.2020.106438

Müller Schmied, H., Adam, L., Eisner, S., Fink, G., Flörke, M., Kim, H., et al. (2016). Variations of global and continental water balance components as impacted by climate forcing uncertainty and human water use. *Hydrology and Earth System Sciences*, *20*(7), 2877–2898. https://doi.org/10.5194/hess-20-2877-2016

NASA. (2021). Lake Mead drops to a record low. Retrieved from https://earthobservatory.nasa.gov/images/148758/lake-mead-drops-to-a-record-low

National Research Council. (2004). *Assessing the national streamflow information program*. National Academies Press 10967. https://doi.org/10.17226/10967

National Weather Service. (2019). Mississippi river flood history 1543-present. Retrieved November 3, 2020, from https://www.weather.gov/lix/ms_flood_history

Nigro, J., Slayback, D., Policelli, F., & Brakenridge, G. R. (2014). NASA/DFO MODIS Near Real-Time (NRT) Global Flood Mapping Product Evaluation of Flood and Permanent Water Detection (Vol. 27).

Omernik, J. M. (1987). Ecoregions of the conterminous United States. *Annals of the Association of American Geographers*, *77*(1), 118–125. https://doi.org/10.1111/j.1467-8306.1987.tb00149.x

Omernik, J. M., & Bailey, R. G. (1997). Distinguishing between watersheds and ecoregions. *Journal of the American Water Resources Association*, *33*(5), 15. https://doi.org/10.1111/j.1752-1688.1997.tb04115.x

Paxton, A., Schoof, J. T., Ford, T. W., & Remo, J. W. F. (2021). Extreme precipitation in the great lakes region: Trend estimation and relation with large-scale circulation and humidity. *Frontiers in Water*, *3*, 782847. https://doi.org/10.3389/frwa.2021.782847

Pekel, J.-F., Cottam, A., Gorelick, N., & Belward, A. S. (2016). High-resolution mapping of global surface water and its long-term changes. *Nature*, *540*(7633), 418–422. https://doi.org/10.1038/nature20584

Perin, V., Tulbure, M. G., Gaines, M. D., Reba, M. L., & Yaeger, M. A. (2021). On-farm reservoir monitoring using Landsat inundation datasets. *Agricultural Water Management*, *246*, 106694. https://doi.org/10.1016/j.agwat.2020.106694

Petrakis, R. E., Soulard, C. E., Waller, E. K., & Walker, J. J. (2021). *National surface water maps using daily MODIS satellite data for the conterminous United States - 2003 to 2019*. U.S. Geological Survey ScienceBase. https://doi.org/10.5066/P9UMFBDE

Pickens, A. H., Hansen, M. C., Hancher, M., Stehman, S. V., Tyukavina, A., Potapov, P., et al. (2020). Mapping and sampling to characterize global inland water dynamics from 1999 to 2018 with full Landsat time-series. *Remote Sensing of Environment*, *243*, 111792. https://doi.org/10.1016/j.rse.2020.111792

Pickens, A. H., Hansen, M. C., Stehman, S. V., Tyukavina, A., Potapov, P., Zalles, V., & Higgins, J. (2022). Global seasonal dynamics of inland open water and ice. *Remote Sensing of Environment*, *272*, 112963. https://doi.org/10.1016/j.rse.2022.112963

Pimentel, D., Houser, J., Preiss, E., White, O., Fang, H., Mesnick, L., et al. (1997). Water resources: Agriculture, the environment, and society. *BioScience*, *47*(2), 97–106. https://doi.org/10.2307/1313020

Poff, N. L., Bledsoe, B. P., & Cuhaciyan, C. O. (2006). Hydrologic variation with land use across the contiguous United States: Geomorphic and ecological consequences for stream ecosystems. *Geomorphology*, *79*(3–4), 264–285. https://doi.org/10.1016/j.geomorph.2006.06.032

Pulwarty, R. S., & Melis, T. S. (2001). Climate extremes and adaptive management on the Colorado River: Lessons from the 1997–1998 ENSO event. *Journal of Environmental Management*, *63*(3), 307–324. https://doi.org/10.1006/jema.2001.0494

Quiring, S. M., & Kluver, D. B. (2009). Relationship between winter/spring snowfall and summer precipitation in the northern Great Plains of North America. *Journal of Hydrometeorology*, *10*(5), 1203–1217. https://doi.org/10.1175/2009JHM1089.1

Rad, A. M., Kreitler, J., & Sadegh, M. (2021). Augmented normalized difference water index for improved surface water monitoring. *Environmental Modelling & Software*, *140*, 105030. https://doi.org/10.1016/j.envsoft.2021.105030

R Core Team. (2020). *R Foundation for Statistical Computing*. Retrieved from https://www.R-project.org/

Richey, A. S., Thomas, B. F., Lo, M., Reager, J. T., Famiglietti, J. S., Voss, K., et al. (2015). Quantifying renewable groundwater stress with GRACE. *Water Resources Research*, *51*(7), 5217–5238. https://doi.org/10.1002/2015WR017349

Richter, B. D., Benoit, K., Dugan, J., Getacho, G., LaRoe, N., Moro, B., et al. (2020). Decoupling urban water use and growth in response to water sarcity. *Water*, *12*(10), 14. https://doi.org/10.3390/w12102868

Schaaf, C. B., Gao, F., Strahler, A. H., Lucht, W., Li, X., Tsang, T., et al. (2002). First operational BRDF, albedo nadir reflectance products from MODIS. *Remote Sensing of Environment*, *83*(1–2), 135–148. https://doi.org/10.1016/S0034-4257(02)00091-3

Schaffer-Smith, D., Swenson, J. J., Barbaree, B., & Reiter, M. E. (2017). Three decades of Landsat-derived spring surface water dynamics in an agricultural wetland mosaic; Implications for migratory shorebirds. *Remote Sensing of Environment*, *193*, 180–192. https://doi.org/10.1016/j.rse.2017.02.016

Schilling, K. E., Jha, M. K., Zhang, Y.-K., Gassman, P. W., & Wolter, C. F. (2008). Impact of land use and land cover change on the water balance of a large agricultural watershed: Historical effects and future directions. *Water Resources Research*, *44*(7). https://doi.org/10.1029/2007WR006644

Seaber, P. R., Kapinos, F. P., & Knapp, G. L. (1987). Hydrologic Unit maps. *U.S. Geological Survey Water-Supply Paper 2294*.

Seager, R., Ting, M., Li, C., Naik, N., Cook, B., Nakamura, J., & Liu, H. (2013). Projections of declining surface-water availability for the southwestern United States. *Nature Climate Change*, *3*(5), 482–486. https://doi.org/10.1038/nclimate1787

Sen, P. K. (1968). Estimates of the regression coefficient based on Kendall's Tau. *Journal of the American Statistical Association*, *63*(324), 1379–1389. https://doi.org/10.1080/01621459.1968.10480934

Senay, G. B., Schauer, M., Friedrichs, M., Velpuri, N. M., & Singh, R. K. (2017). Satellite-based water use dynamics using historical Landsat data (1984–2014) in the southwestern United States. *Remote Sensing of Environment*, *202*, 98–112. https://doi.org/10.1016/j.rse.2017.05.005

Shao, W., & Kam, J. (2020). Retrospective and prospective evaluations of drought and flood. *Science of The Total Environment*, *748*, 141155. https://doi.org/10.1016/j.scitotenv.2020.141155

Shuter, B. J., Minns, C. K., & Fung, S. R. (2013). Empirical models for forecasting changes in the phenology of ice cover for Canadian lakes. *Canadian Journal of Fisheries and Aquatic Sciences*, *70*(7), 982–991. https://doi.org/10.1139/cjfas-2012-0437

Slater, L., & Villarini, G. (2017). Evaluating the drivers of seasonal streamflow in the U.S. Midwest. *Water*, *9*(9), 695. https://doi.org/10.3390/w9090695

Smith, J. A., Cox, A. A., Baeck, M. L., Yang, L., & Bates, P. (2018). Strange floods: The upper tail of flood peaks in the United States. *Water Resources Research*, *54*(9), 6510–6542. https://doi.org/10.1029/2018WR022539

Soulard, C. E., Walker, J. J., & Petrakis, R. E. (2020). Implementation of a surface water extent model in Cambodia using cloud-based remote sensing. *Remote Sensing*, *12*(6), 984. https://doi.org/10.3390/rs12060984

Soulard, C. E., Waller, E. K., Walker, J. J., & Petrakis, R. E. (2021). *DSWEmod surface water map composites generated from daily MODIS images - California*. U.S. Geological Survey data release. https://doi.org/10.5066/P9RVPJWE

Soulard, C. E., Waller, E. K., Walker, J. J., Petrakis, R. E., & Smith, B. W. (2022). DSWEmod — The production of high-frequency surface water map composites from daily MODIS images. *JAWRA Journal of the American Water Resources Association*, 1752–1688. https://doi.org/10.1111/1752-1688.12996

Stehman, S. V., & Foody, G. M. (2019). Key issues in rigorous accuracy assessment of land cover products. *Remote Sensing of Environment*, *231*, 111199. https://doi.org/10.1016/j.rse.2019.05.018

Stephens, T. A., & Bledsoe, B. P. (2020). Low-flow trends at Southeast United States streamflow gauges. *Journal of Water Resources Planning and Management*, *146*(6), 04020032. https://doi.org/10.1061/(ASCE)WR.1943-5452.0001212

Stonestrom, D. A., Scanlon, B. R., & Zhang, L. (2009). Introduction to special section on impacts of land use change on water resources. *Water Resources Research*, *45*(7). https://doi.org/10.1029/2009WR007937

Tamiminia, H., Salehi, B., Mahdianpari, M., Quackenbush, L., Adeli, S., & Brisco, B. (2020). Google Earth Engine for geo-big data applications: A meta-analysis and systematic review. *ISPRS Journal of Photogrammetry and Remote Sensing*, *164*, 152–170. https://doi.org/10.1016/j.isprsjprs.2020.04.001

Thornton, M. M., Shrestha, R., Wei, Y., Thornton, P. E., Kao, S., & Wilson, B. E. (2020). Daymet: Daily surface weather data on a 1-km Grid for North America, version 4. ORNL DAAC. https://doi.org/10.3334/ORNLDAAC/1840

Topp, S. N., Pavelsky, T. M., Dugan, H. A., Yang, X., Gardner, J., & Ross, M. R. V. (2021). Shifting patterns of summer lake color phenology in over 26,000 US lakes. *Water Resources Research*, *57*(5). https://doi.org/10.1029/2020WR029123

Tulbure, M. G., & Broich, M. (2013). Spatiotemporal dynamic of surface water bodies using Landsat time-series data from 1999 to 2011. *ISPRS Journal of Photogrammetry and Remote Sensing*, *79*, 44–52. https://doi.org/10.1016/j.isprsjprs.2013.01.010

Tulbure, M. G., & Broich, M. (2019). Spatiotemporal patterns and effects of climate and land use on surface water extent dynamics in a dryland region with three decades of Landsat satellite data. *Science of the Total Environment*, *658*, 1574–1585. https://doi.org/10.1016/j.scitotenv.2018.11.390

USDA. (2021). National Agriculture Imagery Program (NAIP) imagery. Retrieved from https://www.fsa.usda.gov/programs-and-services/aerial-photography/imagery-programs/naip-imagery/

USGS. (2019). *Landsat dynamic surface water extent (DSWE) product Guide* (No. LSDS-1331). Department of the Interior - U.S. Geological Survey. Retrieved from https://www.usgs.gov/media/files/landsat-dynamic-surface-water-extent-product-guide

USGS. (2020). *Water-year summary for site USGS 07032000* [Dataset]. Retrieved October 28, 2020, from https://waterdata.usgs.gov/nwis/wys_rpt?dv_ts_ids=130707&wys_water_yr=2019&site_no=07032000&agency_cd=USGS&adr_water_years=2015%2C2016%2C2017%2C2018%2C2019&referred_module=

USGS. (2022). National water information System: Web Interface. Retrieved from https://waterdata.usgs.gov/nwis

USGS EROS. (2018). Digital elevation - Shuttle radar topography mission (SRTM) 1 arc-second global. *Earth Resources Observation and Science (EROS) Center*. https://doi.org/10.5066/F7PR7TFT

USGS NWIS. (2022a). USGS 10010000 Great Salt Lake At Saltair Boat Harbor, UT. Retrieved from https://nwis.waterdata.usgs.gov/ut/nwis/uv/?cb_62614=on&format=gif_default&site_no=10010000&period=&begin_date=2003-01-01&end_date=2019-12-31

USGS NWIS. (2022b). USGS 10288500 Walker Lake NR Hawthorne, NV. Retrieved from https://nwis.waterdata.usgs.gov/nv/nwis/uv/?cb_00054=on&cb_00062=on&format=gif_default&site_no=10288500&period=&begin_date=2003-01-01&end_date=2019-12-31

USGS NWIS. (2022c). USGS 10336500 Pyramid Lake NR Nixon, NV. Retrieved from https://waterdata.usgs.gov/nv/nwis/dv?cb_00062=on&format=gif_default&site_no=10336500&referred_module=sw&period=&begin_date=2003-01-01&end_date=2019-12-31

USGS NWIS. (2022d). USGS surface-water data for the nation. Retrieved from https://waterdata.usgs.gov/nwis/sw

Utah Water Science Center. (2021). Great Salt Lake elevations. Retrieved from https://www.usgs.gov/centers/utah-water-science-center/science/great-salt-lake-elevations

Vanderhoof, M. K., Christensen, J., Beal, Y.-J. G., DeVries, B., Lang, M. W., Hwang, N., et al. (2020). Isolating anthropogenic wetland loss by concurrently tracking inundation and land cover disturbance across the Mid-Atlantic region, U.S. *Remote Sensing*, *12*(9), 1464. https://doi.org/10.3390/rs12091464

Villarini, G., Smith, J. A., Baeck, M. L., & Krajewski, W. F. (2011). Examining flood frequency distributions in the Midwest U.S. *JAWRA Journal of the American Water Resources Association*, *47*(3), 447–463. https://doi.org/10.1111/j.1752-1688.2011.00540.x

Villarini, G., Smith, J. A., Serinaldi, F., Ntelekos, A. A., & Schwarz, U. (2012). Analyses of extreme flooding in Austria over the period 1951-2006. *International Journal of Climatology*, *32*(8), 1178–1192. https://doi.org/10.1002/joc.2331

von Storch, H. (1999). Misuses of statistical analysis in climate research. In H. von Storch, & A. Navarra (Eds.), *Analysis of climate variability* (pp. 11–26). Springer Berlin Heidelberg. https://doi.org/10.1007/978-3-662-03744-7_2

Walker, J. J., Petrakis, R. E., & Soulard, C. E. (2020). *Implementation of a surface water extent model using cloud-based remote sensing - code and maps*. U.S. Geological Survey data release. Retrieved from https://www.sciencebase.gov/catalog/item/5e28b8d8e4b0d3f93b05fe4a

Walker, J. J., Soulard, C. E., & Petrakis, R. E. (2020). Integrating stream gage data and Landsat imagery to complete time-series of surface water extents in Central Valley, California. *International Journal of Applied Earth Observation and Geoinformation*, *84*, 101973. https://doi.org/10.1016/j.jag.2019.101973

Waylen, P., Southworth, J., Gibbes, C., & Tsai, H. (2014). Time series analysis of land cover change: Developing statistical tools to determine significance of land cover changes in persistence analyses. *Remote Sensing*, *6*(5), 4473–4497. https://doi.org/10.3390/rs6054473

Webb, B. W., & Nobilis, F. (1995). Long term water temperature trends in Austrian rivers. *Hydrological Sciences Journal*, *40*(1), 83–96. https://doi.org/10.1080/02626669509491392

Williams, A. P., Cook, E. R., Smerdon, J. E., Cook, B. I., Abatzoglou, J. T., Bolles, K., et al. (2020). Large contribution from anthropogenic warming to an emerging North American megadrought. *Science*, *368*(6488), 314–318. https://doi.org/10.1126/science.aaz9600

Wobus, C., Lawson, M., Jones, R., Smith, J., & Martinich, J. (2014). Estimating monetary damages from flooding in the United States under a changing climate. *Journal of Flood Risk Management*, *7*(3), 217–229. https://doi.org/10.1111/jfr3.12043

Wulder, M. A., White, J. C., Loveland, T. R., Woodcock, C. E., Belward, A. S., Cohen, W. B., et al. (2016). The global Landsat archive: Status, consolidation, and direction. *Remote Sensing of Environment*, *185*, 271–283. https://doi.org/10.1016/j.rse.2015.11.032

Xiong, X., Aldoretta, E., Angal, A., Chang, T., Geng, X., Link, D., et al. (2020). Terra MODIS: 20 years of on-orbit calibration and performance. *Journal of Applied Remote Sensing*, *14*(3), 1–16. https://doi.org/10.1117/1.JRS.14.037501

Xiong, X., Angal, A., Twedt, K. A., Link, D., Geng, X., Aldoretta, E., & Mu, Q. (2019). MODIS reflective solar bands on-orbit calibration and performance. *IEEE Transactions on Geoscience and Remote Sensing*, *57*(9), 1–17. https://doi.org/10.1109/TGRS.2019.2905792

Yamazaki, D., Trigg, M. A., & Ikeshima, D. (2015). Development of a global ~90m water body map using multi-temporal Landsat images. *Remote Sensing of Environment*, *171*, 337–351. https://doi.org/10.1016/j.rse.2015.10.014

Yue, S., Pilon, P., & Cavadias, G. (2002). Power of the Mann–Kendall and Spearman's rho tests for detecting monotonic trends in hydrological series. *Journal of Hydrology*, *259*(1–4), 254–271. https://doi.org/10.1016/S0022-1694(01)00594-7

Yue, S., & Wang, C. Y. (2002). Applicability of pre-whitening to eliminate the influence of serial correlation on the Mann-Kendall test: Technical Note. *Water Resources Research*, *38*(6), 4-1–4–7. https://doi.org/10.1029/2001WR000861

Zhang, Y., Song, C., Band, L. E., Sun, G., & Li, J. (2017). Reanalysis of global terrestrial vegetation trends from MODIS products: Browning or greening? *Remote Sensing of Environment*, *191*, 145–155. https://doi.org/10.1016/j.rse.2016.12.018

Zhou, Y., Dong, J., Xiao, X., Xiao, T., Yang, Z., Zhao, G., et al. (2017). Open surface water mapping algorithms: A comparison of water-related spectral indices and sensors. *Water*, *9*(4), 256. https://doi.org/10.3390/w9040256

Zou, Z., Xiao, X., Dong, J., Qin, Y., Doughty, R. B., Menarguez, M. A., et al. (2018). Divergent trends of open-surface water body area in the contiguous United States from 1984 to 2016. *Proceedings of the National Academy of Sciences*, *115*(15), 3810–3815. https://doi.org/10.1073/pnas.1719275115